


The Kir2.1^{E299V} mutation increases atrial fibrillation vulnerability while protecting the ventricles against arrhythmias in a mouse model of short QT syndrome type 3

Ana I. Moreno-Manuel ¹, Álvaro Macías ^{1*}, Francisco M. Cruz ^{1*}, Lilian K. Gutiérrez¹, Fernando Martínez^{1,2}, Andrés González-Guerra^{1†}, Isabel Martínez Carrascoso¹, Francisco José Bermúdez-Jimenez^{1,3}, Patricia Sánchez-Pérez¹, María Linarejos Vera-Pedrosa¹, Juan Manuel Ruiz-Robles¹, Juan A. Bernal ^{1,2*}, and José Jalife ^{1,2,4}

¹Centro Nacional de Investigaciones Cardiovasculares (CNIC), Melchor Fernández Almagro 3, 28029 Madrid, Spain; ²CIBER de Enfermedades Cardiovasculares (CIBERCV), Madrid, Spain; ³Department of Cardiology, Hospital Universitario Virgen de las Nieves, 18014 Granada, Spain; and ⁴Departments of Internal Medicine and Molecular and Integrative Physiology, Center for Arrhythmia Research, University of Michigan, Ann Arbor, MI 4810, USA

Received 4 July 2023; revised 24 October 2023; accepted 12 December 2023; online publish-ahead-of-print 23 January 2024

Time for primary review: 55 days

Aims Short QT syndrome type 3 (SQT3) is a rare arrhythmogenic disease caused by gain-of-function mutations in *KCNJ2*, the gene coding the inward rectifier potassium channel Kir2.1. We used a multidisciplinary approach and investigated arrhythmogenic mechanisms in an *in-vivo* model of *de-novo* mutation Kir2.1^{E299V} identified in a patient presenting an extremely abbreviated QT interval and paroxysmal atrial fibrillation.

Methods and results We used intravenous adeno-associated virus-mediated gene transfer to generate mouse models, and confirmed cardiac-specific expression of Kir2.1^{WT} or Kir2.1^{E299V}. On ECG, the Kir2.1^{E299V} mouse recapitulated the QT interval shortening and the atrial-specific arrhythmia of the patient. The PR interval was also significantly shorter in Kir2.1^{E299V} mice. Patch-clamping showed extremely abbreviated action potentials in both atrial and ventricular Kir2.1^{E299V} cardiomyocytes due to a lack of inward-going rectification and increased I_{K1} at voltages positive to −80 mV. Relative to Kir2.1^{WT}, atrial Kir2.1^{E299V} cardiomyocytes had a significantly reduced slope conductance at voltages negative to −80 mV. After confirming a higher proportion of heterotetrameric Kir2.x channels containing Kir2.2 subunits in the atria, *in-silico* 3D simulations predicted an atrial-specific impairment of polyamine block and reduced pore diameter in the Kir2.1^{E299V}-Kir2.2^{WT} channel. In ventricular cardiomyocytes, the mutation increased excitability by shifting I_{Na} activation and inactivation in the hyperpolarizing direction, which protected the ventricle against arrhythmia. Moreover, Purkinje myocytes from Kir2.1^{E299V} mice manifested substantially higher I_{Na} density than Kir2.1^{WT}, explaining the abbreviation in the PR interval.

Conclusion The first *in-vivo* mouse model of cardiac-specific SQT3 recapitulates the electrophysiological phenotype of a patient with the Kir2.1^{E299V} mutation. Kir2.1^{E299V} eliminates rectification in both cardiac chambers but protects against ventricular arrhythmias by increasing excitability in both Purkinje-fiber network and ventricles. Consequently, the predominant arrhythmias are supraventricular likely due to the lack of inward rectification and atrial-specific reduced pore diameter of the Kir2.1^{E299V}-Kir2.2^{WT} heterotetramer.

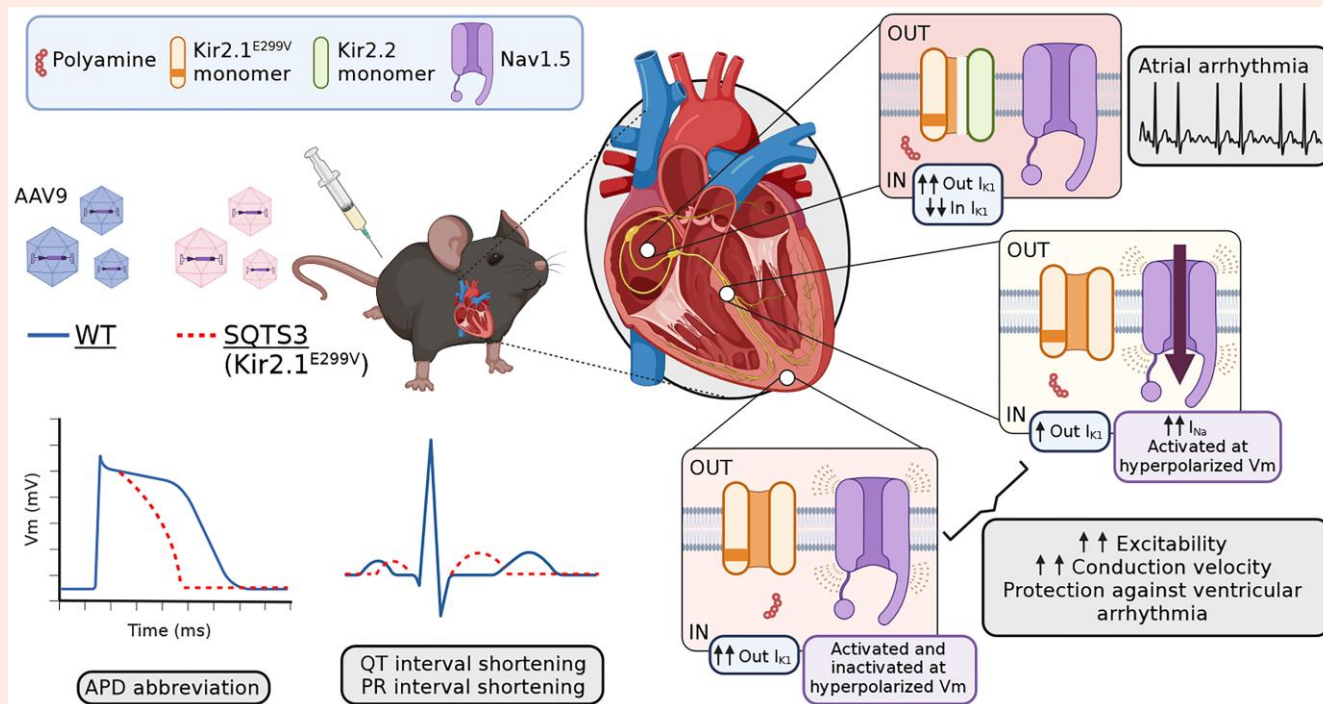
* Corresponding author. Tel: +34 91 453 12 00 (Ext. 3307); fax: +34 91 453 12 65, E-mail: jabernal@cnic.es (J.A.B.); Tel: +34 91 453 12 00 (Ext. 4311); fax: +34 91 453 12 65, E-mail: alvaromacias@cnic.es (A.M.); Tel: +34 91 453 12 00 (Ext. 4308); fax: +34 91 453 12 65, E-mail: fmcruz@cnic.es (F.M.C.)

† Present address: European Molecular Biology Laboratory (EMBL), 00015, Monterotondo, Lazio, Italy.

© The Author(s) 2024. Published by Oxford University Press on behalf of the European Society of Cardiology.

This is an Open Access article distributed under the terms of the Creative Commons Attribution License (<https://creativecommons.org/licenses/by/4.0/>), which permits unrestricted reuse, distribution, and reproduction in any medium, provided the original work is properly cited.

Graphical Abstract



Keywords

Electrocardiogram • Action potential duration • Excitability • Kir2.1-NaV1.5 channelosome • Atrial and ventricular arrhythmias

1. Introduction

Short QT syndrome (SQTs) is a rare, highly lethal inheritable disease characterized by an abnormally short QT interval on the electrocardiogram (ECG) and an increased risk for atrial- and ventricular fibrillation (AF/VF), and sudden cardiac death (SCD).^{1–3} To date, less than 250 cases in nearly 150 families have been diagnosed worldwide, all during the last decades.^{1,3} Despite their heterogeneous phenotype, SQTs patients can manifest palpitations, cardiac arrest, syncope, or AF.⁴

SQTs is considered a disease with an autosomal dominant inheritance. However, only 20–30% of patients with SQTs have an identifiable mutation.^{5,6} To date, only four genes encoding potassium channels (*KCNQ1*, *KCNH2*, and *KCNJ2*) and the chloride-bicarbonate exchanger *AE3* (*SLC4A3*) have been clearly associated with pathogenic SQTs.^{7–9} However, we still lack detailed information about the factors responsible for the relative malignancy and specific arrhythmogenic mechanisms of each of the known mutations.

SQTs type 3 [SQTs3 (OMIM 609622)] is caused by *KCNJ2* gain-of-function mutations.^{10,11} The *KCNJ2* gene encodes the strong inward rectifier potassium channel Kir2.1 responsible for I_{K1}.¹² Outward currents through Kir2.x channels regulate the resting membrane potential (RMP), the threshold for excitation, and the final phase of action potential (AP) repolarization.^{12,13} Among the SQTs3 causative mutations, Kir2.1^{E299V} (c.896A > T) was identified in an 11-year-old boy with an extremely abbreviated QT interval (200 ms) and paroxysmal AF, but without ventricular arrhythmias despite mild left ventricular dysfunction (possibly due to the rapid AF rate).¹⁴ The defects caused by Kir2.1^{E299V} were studied in a heterologous expression system.¹⁴ While valid, the approach precluded investigating arrhythmogenic mechanisms in the complex cardiac environment. Importantly, glutamic acid at position 299 is highly conserved

in Kir2.1 channels among species.¹⁰ It is located at the cytoplasmic domain and, together with other negatively charged residues, forms the inner vestibule of the channel pore, which determines the strength of inward I_{K1} rectification.^{15,16} Inward rectification is attributed to a voltage-dependent blockade of outward current by internal Mg²⁺ and polyamines (spermine, spermidine, and putrescine).¹⁷ In Kir2.1 channels, rectification is regulated by two different negatively charged regions, one in the transmembrane domain, involving D172, and the other in the cytoplasmic region, involving E224, D255, D259, and E299.¹⁸ Polyamines are important in aging, cancer, and other diseases, but induction of inward rectification is likely their most important function.¹⁹ However, to our knowledge, polyamines have never been used to investigate SQTs3 mechanisms or SCD, and it is unknown whether they have a role in linking channel dysfunction to arrhythmias.

On the other side, Kir2.1 interacts with the cardiac voltage-gated sodium channel Na_v1.5 forming channelosomes from early stages of their common trafficking pathway, and both channels regulate each other's function.²⁰ Trafficking-deficient mutations in one of these channels reduce the surface expression and current density of the other.^{21–25} However, it is unknown whether gain-of-function mutations in one or the other channel modify such interactions or result in unforeseen electrical remodeling mediated by changes in other interacting proteins.

Here, we report on the first *in-vivo* mouse model of cardiac-specific SQTs3 mimicking the electrophysiological phenotype of a patient with the Kir2.1^{E299V} mutation. A clear consequence of the mutation was the extreme atrial and ventricular AP and QT interval shortening due to the loss of polyamine-mediated inward-going rectification. However, unlike the atria, the gain-of-function of this Kir2.1 mutation increased excitability and protected against arrhythmia inducibility in the ventricles. Therefore, like in the patient, the predominant arrhythmias were supraventricular, including atrial tachycardia and AF.

2. Methods

Detailed descriptions are provided in the [Supplementary material online](#).

2.1 Study approval

All experimental procedures using animals conformed to EU Directive 2010/63EU and Recommendation 2007/526/EC, enforced in Spanish law under *Real Decreto 53/2013*. They were approved by the local ethics committees and the Animal Protection Area of the Comunidad Autónoma de Madrid (PROEX 111.4/20).

2.2 Mice

Four-week-old C57BL/6J male mice were obtained from Charles River Laboratories. Mice were reared and housed in accordance with institutional guidelines and regulations.

2.3 Adeno-associated virus (AAV) production, injection, and mouse models generation

Vectors encoding wildtype (WT) Kir2.1 (Kir2.1^{WT}) or the SQT3S Kir2.1 mutant (Kir2.1^{E299V}) were packaged into adeno-associated virus (AAV) serotype 9 (AAV9) capsids.^{26–29} After anaesthesia (Ketamine 60 mg/kg and Xylazine 20 mg/kg i.p.), 4- to 5-week-old mice were administered 3.5×10^{10} viral genomes (vg) per animal i.v. in a final volume of 50 μ L.^{26,30} Mice were used for experiments at 15–25 weeks of age.

2.4 Echocardiography

Mice were anaesthetised with 0.5–2% Isoflurane in oxygen, and placed on a 37°C heating platform in the supine position. Transthoracic echocardiography was performed blindly by an expert operator using a high-frequency ultrasound system (Vevo 2100, VisualSonics Inc., Canada) with a 40-MHz linear probe, and analyzed blindly as described (see [Supplementary material online](#)).

2.5 Surface ECG recordings

Mice were anaesthetised with 0.8–1% Isoflurane in oxygen. A subcutaneous 23-gauge needle electrode connected to an MP36R amplifier (BIOPAC Systems) was attached to each limb, and six-lead surface ECGs were recorded for 5 min. We analyzed blindly the recordings using AcqKnowledge 4.1 software.

2.6 In-vivo intracardial electrophysiology

After anaesthesia (Ketamine 60 mg/kg and Xylazine 20 mg/kg i.p.), an octopolar catheter (Science) was inserted in the heart through the jugular vein.^{31,32} Refractory periods and arrhythmia inducibility were assessed in control and mutant mice.

2.7 Optical mapping in isolated hearts

Optical mapping experiments in Kir2.1^{WT} and Kir2.1^{E299V} mice were carried out blindly as previously described.³³

2.8 Atrial and ventricular cardiomyocyte isolation

After cervical dislocation, the mouse heart was mounted on a Langendorff-perfusion apparatus, and the aorta was retrogradely perfused, as per Macías et al.³⁴

2.9 HEK-293 T/HEK-Na_v1.5 cells culture and transfection

We maintained human embryonic kidney (HEK) 293 T (ATCC number CRL-3216) and HEK-Na_v1.5 cells (kindly provided by Dr. Carmen

Valenzuela, CSIC-UAM Madrid) in Dulbecco's modified eagle medium supplemented with 10% fetal bovine serum, 1% penicillin/streptomycin and L-glutamine. We used 0.2% Zeocin to select Na_v1.5 containing cells.³⁵ We transfected these cells using JetPRIME transfection reagent (Polyplus).

2.10 Patch-clamping of cardiomyocytes and HEK cells

Whole-cell (current- and voltage-clamp), inside-out patch-clamping, and data analysis procedures were as described previously^{22–24,36,37} (see [Supplementary material online](#)). External and internal solutions are listed in [Supplementary material online, Table S1](#).^{24,38}

2.11 Immunohistochemistry/fluorescence

We used goat polyclonal anti-Tomato antibody (Sicgen, AB8181-200) and hematoxylin-eosin in 5–7 μ m-thick sections to analyze blindly mouse heart tissue structure and the level of AAV9 infection.

2.12 Immunofluorescence

Isolated cardiomyocytes were processed and incubated with primary and secondary antibodies specified in [Supplementary material online, Tables S2 and S3](#). Images were acquired with a Leica SP8 confocal microscope.

2.13 Western blot and membrane fractionation

Whole hearts or specific cardiac chambers from control and mutant mice were excised and lysed using ice-cold radioimmunoprecipitation assay buffer. To measure Kir2.1 membrane protein levels in mouse cardiomyocytes, we followed manufacturer's instructions (Abcam, ab65400). 25–80 μ g of protein resolved in 5–10% SDS-PAGE gels. Antibodies are listed in [Supplementary material online, Tables S4 and S5](#).

2.14 Quantitative real-time PCR (qRT-PCR)

Heart samples from uninfected, AAV9-Tomato, AAV9-Kir2.1^{WT}, and AAV9-Kir2.1^{E299V} mice were homogenized for RNA extraction. The resultant cDNA was analyzed by qRT-PCR using specific primers to amplify the desired genetic products (see [Supplementary material online, Table S6](#)).

2.15 In silico modelling

Protein data bank templates were generated from the Fast-All (FASTA) sequences of Kir2.1, Kir2.2, and Kir2.3.³⁹ Comparative modelling was performed using the ROSETTA framework.⁴⁰ The target sequences (FASTA format) including the E299V mutation were threaded onto the three-dimensional backbone of the template structures according to a multi-sequence alignment. See details in the [Supplementary material online](#).

2.16 Statistical analysis

We used GraphPad Prism software versions 7.0 and 8.0, normal (Gaussian) distribution analysis (Shapiro–Wilk test), Grubb's test for outliers, and Student's t-test for comparisons. For non-Gaussian distributions, we applied the nonparametric Mann–Whitney test. We used one- or two-way analysis of variance (ANOVA) for comparison among more than two groups. Data are expressed as mean \pm SEM, and differences are considered significant at $P < 0.05$ (* $P < 0.05$; ** $P < 0.01$; *** $P < 0.001$; **** $P < 0.0001$). Note that 'N' refers to the number of mice or transfections used and 'n' to the number of cells analyzed per mice/transfection.

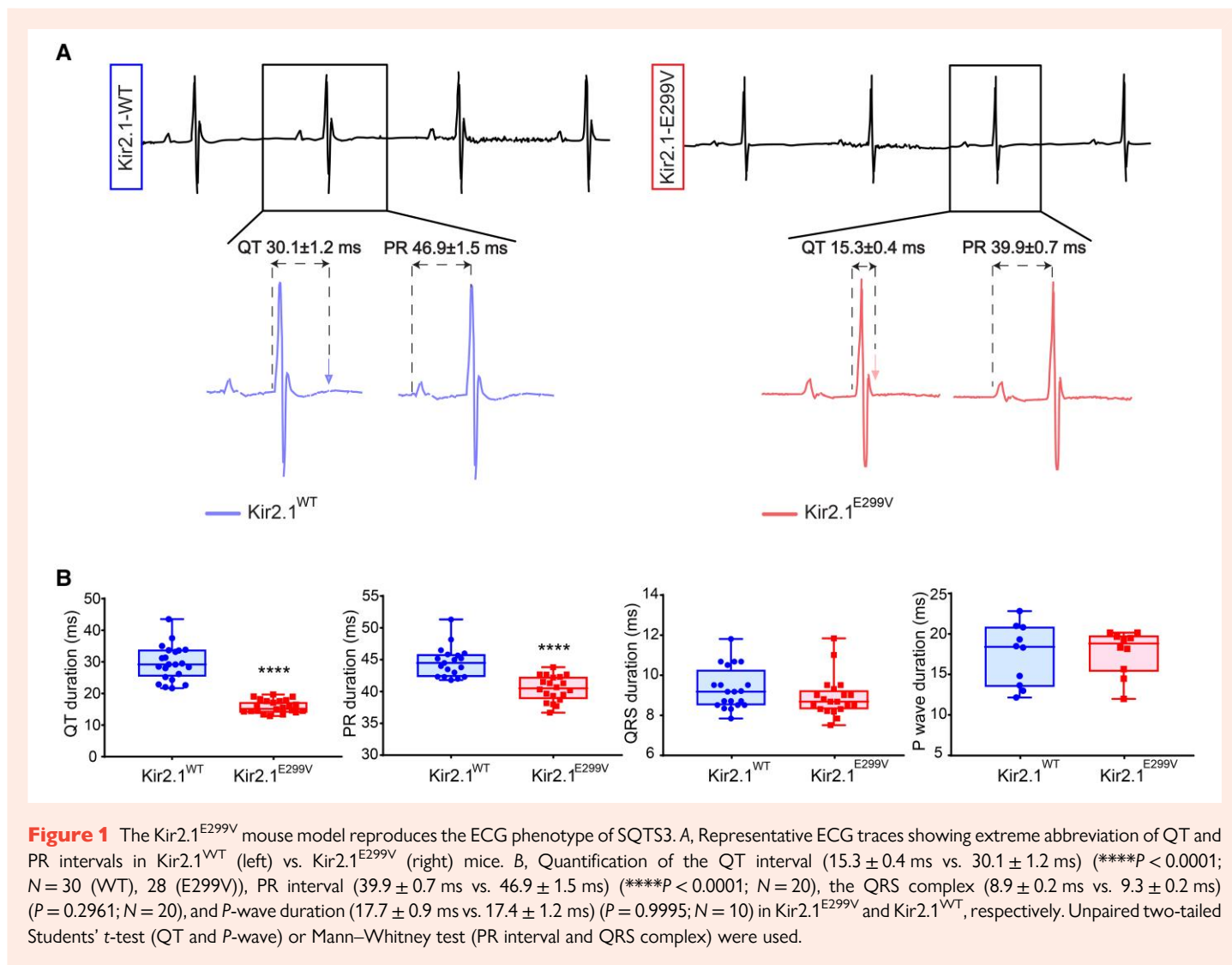


Figure 1 The Kir2.1^{E299V} mouse model reproduces the ECG phenotype of SQT3S. **A**, Representative ECG traces showing extreme abbreviation of QT and PR intervals in Kir2.1^{WT} (left) vs. Kir2.1^{E299V} (right) mice. **B**, Quantification of the QT interval (15.3 ± 0.4 ms vs. 30.1 ± 1.2 ms) (****P < 0.0001; N = 30 (WT), 28 (E299V)), PR interval (39.9 ± 0.7 ms vs. 46.9 ± 1.5 ms) (****P < 0.0001; N = 20), the QRS complex (8.9 ± 0.2 ms vs. 9.3 ± 0.2 ms) (P = 0.2961; N = 20), and P-wave duration (17.7 ± 0.9 ms vs. 17.4 ± 1.2 ms) (P = 0.9995; N = 10) in Kir2.1^{E299V} and Kir2.1^{WT}, respectively. Unpaired two-tailed Student's t-test (QT and P-wave) or Mann–Whitney test (PR interval and QRS complex) were used.

3. Results

3.1 Validation and characterization of mouse models

We generated mouse models of SQT3S using AAV9. We confirmed cardiac-specific expression of Kir2.1^{WT} or Kir2.1^{E299V} by the fluorescence emitted by the tdTomato reporter in the AAV construct, totally absent in uninfected hearts (see [Supplementary material online, Figure S1A and B](#)). Immunohistochemistry of tdTomato in ventricular and atrial slices confirmed global AAV9 infection of ~95%, with ~50% cardiomyocytes expressing 2–4vg/cell (see [Supplementary material online, Figure S1C–F](#)), as reported previously.²⁶ We also confirmed the infection of cardiac conduction system cells using Cx40^{GFP} transgenic mice (see [Supplementary material online, Figure S1G](#)). Haematoxylin-Eosin staining and echocardiographic analysis confirmed the unaffected structure and contractile function in either Kir2.1^{WT} or Kir2.1^{E299V} hearts (see [Supplementary material online, Figure S1C and S2](#)).

qRT-PCR of the transgene demonstrated that, unlike the uninfected group, hearts from Kir2.1^{WT} and Kir2.1^{E299V} mice amplified the human *KCNJ2* (see [Supplementary material online, Figure S3A](#)). We also ensured that genetic haploinsufficiency did not operate after expression in *trans* of Kir2.1^{WT} and Kir2.1^{E299V}. We confirmed that WT and mutant transcripts did not disturb endogenous Kir2.1–3 mRNA levels (see

[Supplementary material online, Figure S3A](#)). As described,⁴¹ the Kir2.3 isoform is not predominant in murine myocardium, so the *KCNJ4* mRNA was undetectable in our experiments. Despite the amplification of the human *KCNJ2* confirmed by qRT-PCR, total protein levels from the whole hearts of uninfected, Kir2.1^{WT} and Kir2.1^{E299V} were very similar (see [Supplementary material online, Figure S3B](#), left panel, and [Supplementary material online, Figure S4](#)). Endogenous regulatory mechanisms keep Kir2.1 translation at the same levels as when there is no infection, without overexpression in the generated models. Surface membrane Kir2.1 levels in Kir2.1^{WT} and Kir2.1^{E299V} hearts were also similar to each other, so the gain-of-function caused by the E299V mutation was not due to a higher protein expression (see [Supplementary material online, Figure S3B](#), right panel, and [Supplementary material online, Figure S4](#)). Kir2.1 channels placed at the membrane present three bands on western blot likely due to their different glycosylation levels depending on the trafficking pathway.²³ Therefore, since AAV9-Kir2.1^{WT} did not alter the Kir2.1 total expression and represented an infected control, all subsequent experiments were conducted in Kir2.1^{E299V} animals and compared with Kir2.1^{WT} controls.

3.2 Kir2.1^{E299V} mice have an extremely short QT interval

Under basal conditions, both the non-corrected and the corrected QT (QTc) intervals were significantly shorter in Kir2.1^{E299V} than in Kir2.1^{WT}

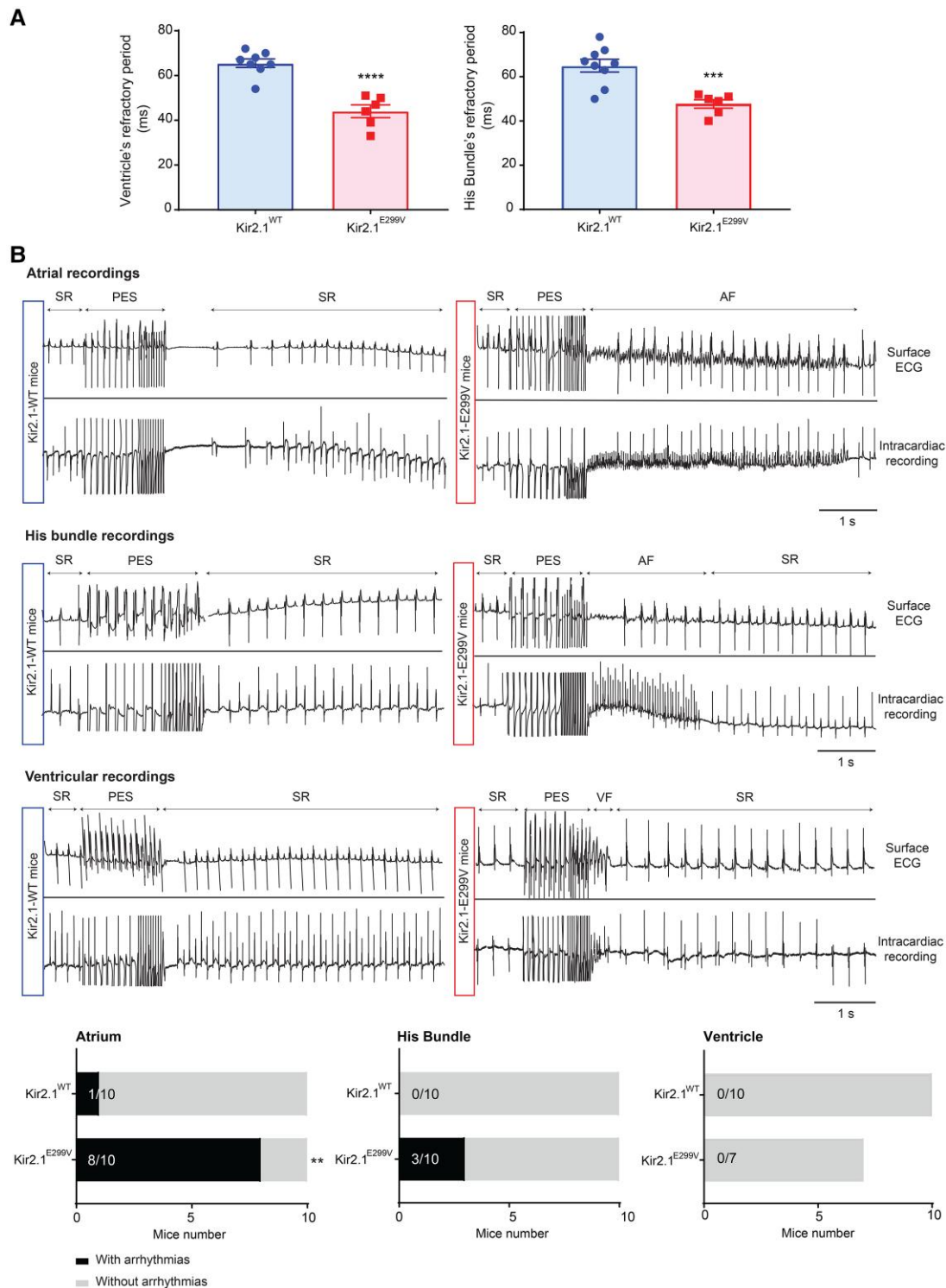


Figure 2 Kir2.1^{E299V} mice have a short refractory period and are highly inducible for atrial arrhythmias. **A**, Ventricular refractory period of Kir2.1^{WT} (N = 8) and Kir2.1^{E299V} (N = 6) (65.5 ± 1.9 ms and 44 ± 2.8 ms, respectively; ****P < 0.0001). His bundle stimulation yielded a refractory period of 65 ± 2.9 ms in Kir2.1^{WT} vs. 47.7 ± 1.9 ms in Kir2.1^{E299V} (**P = 0.0006; N = 9 (WT), 6 (E299V)). **B**, Top, Simultaneous surface ECG and intracardiac recordings from right atrium, His bundle, and ventricle before, during, and after PES protocols. Sinus rhythm (SR), PES, and atrial and ventricular fibrillation (AF, VF) are indicated as corresponded in the traces. Bottom, quantification of atrial tachycardia or AF events lasting >1 s after atrial stimulation in left (1 out of 10 in Kir2.1^{WT} mice, and 8 out of 10 in Kir2.1^{E299V}) (**P = 0.0055; N = 10), His bundle stimulation in the middle (only 3 out of 10 Kir2.1^{E299V}), and ventricular stimulation in right. Unpaired 2-tailed Student's *t*-test (refractory periods) and Fisher's exact test (presence/absence arrhythmias) were applied.

animals (Figure 1A, and Supplementary material online, Figures S5 and S6). The PR interval was also significantly shorter in mutant than WT animals. We used isoproterenol (ISO, 5 mg/kg) to study the response of our models to a stress situation in which the heart rate increases. ISO prolonged the QT interval in Kir2.1^{E299V} to levels similar to Kir2.1^{WT}, but the PR interval continued to reduce in mutant mice (see Supplementary material online, Figure S7A). Both P-wave duration and QRS complex were similar in both groups at baseline, although the QRS tended to be shorter in mutant animals (Figure 1B). Notably, i.p. administration of ISO further shortened the QRS in Kir2.1^{E299V} mice making it significantly different from WT (see Supplementary material online, Figure S7A). Together these data indicated that, in addition to the QT abbreviation characteristic of SQT3, Kir2.1^{E299V} animals had increased atrio-ventricular (AV) and intraventricular conduction velocities (CV), particularly in the presence of ISO.

Chloroquine and flecainide inhibit I_{Kr} and may be beneficial for atrial arrhythmia in patients carrying the Kir2.1^{E299V} mutation.⁴² Chloroquine selectively blocks Kir2.1 channels at <10 μ M.^{43–46} In Kir2.1^{E299V} mice, chloroquine (40 mg/Kg corresponding to <10 μ M in blood when administered i.p.^{47–49}) induced an initial rapid prolongation (<1 min) that brought the QT interval to the Kir2.1^{WT} mouse level. Unfortunately, there was a constant and progressive QT prolongation over a 40-min period in both groups. Chloroquine also prolonged the PR and QRS intervals to non-physiologic durations (see Supplementary material online, Figure S7B), highlighting the potential risk of using chloroquine to treat SQT3 patients. To study if flecainide could normalize the ECG values in Kir2.1^{E299V} animals, we tested the response of both mouse models to this class 1c antiarrhythmic drug (20 mg/kg). Flecainide blocks the cardiac sodium channel and has other effects on excitation–contraction coupling and potassium channels.^{50–52} As demonstrated in Supplementary material online, Figure S7C, flecainide produced a relatively rapid but transient prolongation in the QT interval of the Kir2.1^{WT} mice, but had no effect whatsoever on the QT interval of Kir2.1^{E299V} mice. In contrast, the drug gradually prolonged the PR and QRS intervals over a 6-min period in both groups. In summary, unlike flecainide, chloroquine effectively prolongs the QT interval. However, the effects of both drugs on AV and intraventricular conduction make them unlikely candidates for antiarrhythmic therapy in SQT3 patients. The beneficial effects of these drugs would not be reflected in mice because their hearts do not express I_{Kr} .

3.3 Kir2.1^{E299V} mouse hearts have shorter refractory periods than WT and are highly inducible for atrial but not ventricular arrhythmias

We measured refractory periods in both mouse groups by stimulating the His bundle (localized as described in Alanis et al.⁵³; see Supplementary material online, Figure S8) or the right ventricle (RV) on intracardiac programmed stimulation experiments. In Kir2.1^{E299V} mice, the His bundle and the RV refractory periods were 26.6% and 32.8% shorter than control, respectively (Figure 2A), which was consistent with the reduced QT interval in the SQT3 animals.

To test the susceptibility of the SQT3 model to AF and ventricular tachycardia/fibrillation (VT/VF), we performed intracardiac pacing experiments in both groups of mice by applying an S1-S2 train of 10 and 20 Hz (see Supplementary material online, Extended Materials and Methods). Arrhythmia episodes lasting >1 s in atria were higher in mutant animals compared to control. While only 1/10 Kir2.1^{WT} animals were inducible, 8/10 Kir2.1^{E299V} mice manifested atrial tachycardia or >1 s AF episodes (Figure 2B). As shown in Supplementary material online, Figure S9, 9/10 Kir2.1^{E299V} animals manifested >500 ms atrial arrhythmias episodes.

No Kir2.1^{WT} and only 3/10 Kir2.1^{E299V} animals were inducible for >1 s arrhythmias (Figure 2B) and >500 ms episodes (see Supplementary material online, Figure S9) by His bundle stimulation.

On ventricular stimulation, none of the animals were inducible for arrhythmias lasting >1 s, regardless of genotype (Figure 2B). However, 3/7

Kir2.1^{E299V} mice had >500 ms ventricular episodes (see Supplementary material online, Figure S9).

Even when we stimulated the RV or His bundle of Kir2.1^{E299V} mice, the main type of arrhythmia triggered was AF, as 40% mutant animals yielded atrial arrhythmias when stimulating the RV. Similarly, 60% of Kir2.1^{E299V} animals manifested AF upon His bundle stimulation. Altogether, the vast majority of inducible arrhythmias in the Kir2.1^{E299V} mice were atrial, and of these, the most common was AF. To rule out possible structural alterations underlying the atrial-specific arrhythmia inducibility, we analyzed histologically the atria of WT and mutant animals. We saw no differences in size, wall thickness, or fibrosis (see Supplementary material online, Figure S10).

3.4 Action potential duration (APD) is extremely brief in both atrial and ventricular cardiomyocytes of Kir2.1^{E299V} mice

Despite their extremely short QT interval and ventricular refractory period, Kir2.1^{E299V} mice are much less susceptible to ventricular than atrial arrhythmias. This fact leads to the question of whether the mutation results in a more severe electrical phenotype in atrial than ventricular cardiomyocytes. We, therefore, conducted whole-cell current-clamp experiments to measure the AP characteristics. Clearly, the mutation consistently and significantly abbreviated the atrial action potential duration (APD) at all levels and frequencies studied (Figure 3A, Supplementary material online, Figure 11A and Table S7). As shown in Figure 3Bi-iii, the ventricular APDs in Kir2.1^{E299V} cardiomyocytes were also abbreviated to similar levels as the mutant atrial APDs (see Supplementary material online, Table S8). The significant shortening of both Kir2.1^{E299V} atrial and ventricular APDs was independent of the stimulation frequency and did not vary too much as they increased. As seen in Figure 3Aiv-V and Biv-V, and Supplementary material online, Figure S11, neither RMP, dV/dt, or AP amplitude (APA) were affected in either chamber. Therefore, while APD was the only parameter modified, it did not explain the significantly different atrial vs. ventricular arrhythmia inducibility caused by the mutation.

3.5 I_{K1} is differently affected in atrial vs. ventricular Kir2.1^{E299V} cardiomyocytes

We conducted whole-cell voltage-clamp experiments in atrial and ventricular Kir2.1^{WT} and Kir2.1^{E299V} cardiomyocytes to compare their respective barium-sensitive inward rectifier (I_{K1}) current/voltage (IV) relationships. In Figure 4, Kir2.1^{E299V} cardiomyocytes from both chambers showed a clear increase in I_{K1} outward current due to loss of inward-going rectification. The outward I_{K1} increase was the mechanism that caused significant APD abbreviation at all the stimulation frequencies in cardiomyocytes from both chambers of the Kir2.1^{E299V} mice (Figure 3A and B). However, there was an important difference in the effect of the mutation on the I_{K1} IV relation of atrial vs. ventricular cardiomyocytes. While in atrial Kir2.1^{E299V} cardiomyocytes inward I_{K1} was significantly reduced at voltages negative to -80 mV (Figure 4A), in the ventricles the inward currents were similar in these ranges of voltage in both genotypes (Figure 4B). In other words, inward rectification is absent in both atrial and ventricular Kir2.1^{E299V} cardiomyocytes, but the reduction in the slope conductance of the inward I_{K1} is atrial-specific. This significantly reduced slope conductance relative to WT is likely to predispose the mouse atria to an arrhythmic phenotype.

We used *in-silico* modelling to investigate the mechanism of the absence of inward-going rectification in atrial and ventricular Kir2.1^{E299V} cardiomyocytes. First, we determined structural changes in the ventricular isoforms of Kir2.1^{WT} homotetramers (4 Kir2.1^{WT} subunits) and Kir2.1^{WT}-Kir2.1^{E299V} heterotetramers (2 Kir2.1^{WT} plus 2 Kir2.1^{E299V} subunits). We observed that mutant heterotetrameric conformations undergo conformational changes, particularly on the lateral chains (Root mean square deviation value of 4.081Å when comparing Kir2.1^{WT}-Kir2.1^{E299V} vs. Kir2.1^{WT}). From the stability point of view, all the models were stable

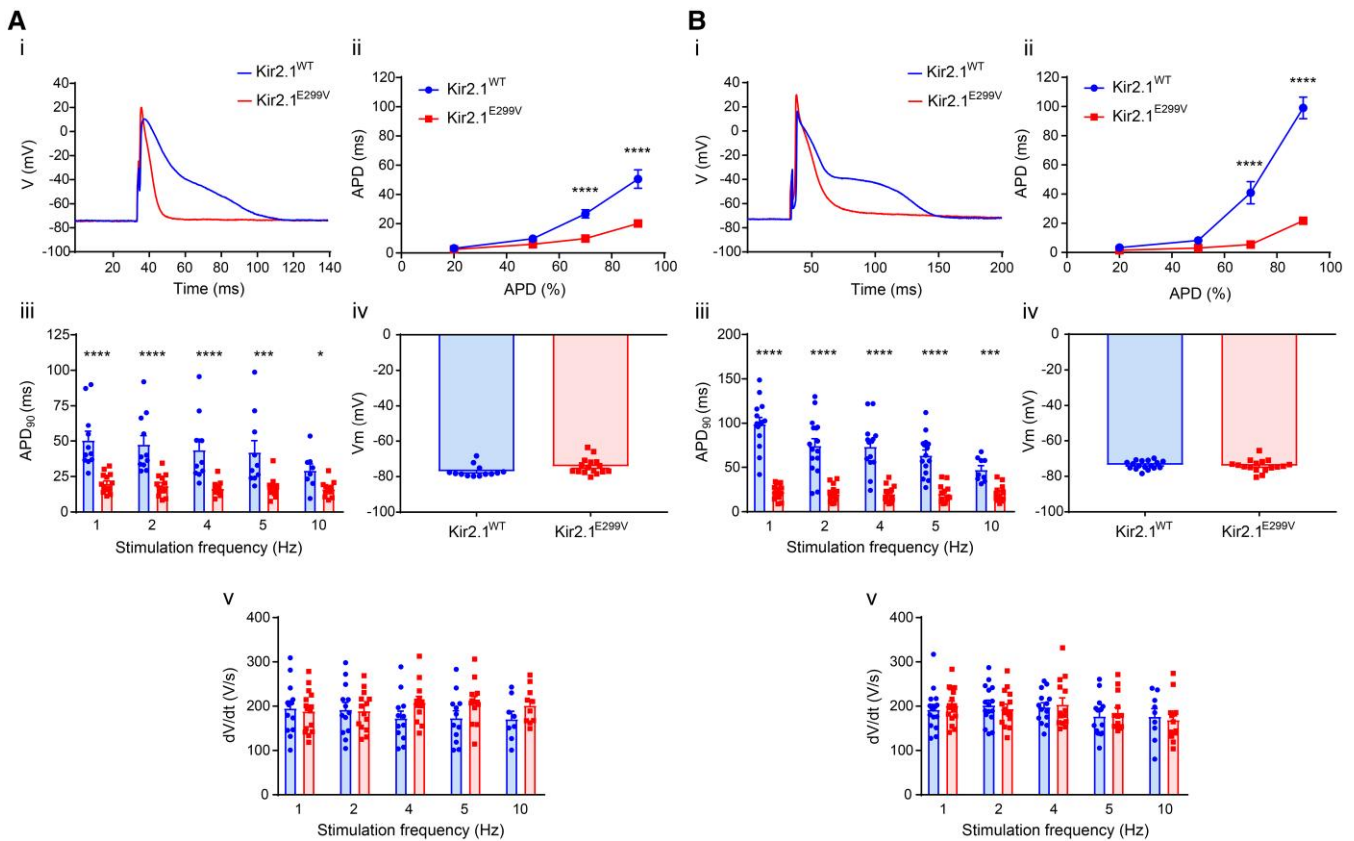


Figure 3 APD is reduced in the atria and ventricles of Kir2.1^{E299V} mice. Electrophysiological characterization of AP from Kir2.1^{WT} and Kir2.1^{E299V}. **A**, Atrial cardiomyocytes. Kir2.1^{WT} ($N = 3$; $n = 8-13$) and Kir2.1^{E299V} ($N = 3$; $n = 10-16$). **B**, Ventricular cardiomyocytes. Kir2.1^{WT} ($N = 3$; $n = 9-17$) and Kir2.1^{E299V} ($N = 3$; $n = 12-17$). Different panels in both regions show representative APs recorded at 1 Hz (i), and APDs at 20, 50, 70 (**** $P < 0.0001$) and 90% (**** $P < 0.0001$) of repolarization for 1 Hz pacing (ii). APD₉₀ at 1, 2, 4, 5, and 10 Hz is shown in panels iii (**** $P < 0.0001$, *** $P < 0.001$, * $P < 0.05$). The RMP for each type of cardiomyocyte (panels iv) and the maxim upstroke velocity (dV/dt_{max}) (panels v) are shown. Unpaired two-tailed Student's *t*-test or Mann-Whitney test were applied.

with very negative values of energy: Kir2.1^{WT} -4801.404 Rosseta Energy Units (REU) and Kir2.1^{WT}-Kir2.1^{E299V} -5234.111 REU.

3.6 K⁺ ions pass more efficiently through the Kir2.1^{WT}-Kir2.1^{E299V} channel structure

Compared with Kir2.1^{WT}, the cytoplasmic pore diameter of the predominant mutant isoform in the ventricles, Kir2.1^{WT}-Kir2.1^{E299V}, was substantially modified by rearrangement of the side chains of the residues lining the pore (Figure 5A, blue dashed arrows). On the other hand, while the transmembrane pore region did not show any appreciable differences between models, the extracellular pore region of the heterotetrameric Kir2.1^{WT}-Kir2.1^{E299V} channel underwent significant expansion and became more hydrophilic compared to the homomeric Kir2.1^{WT} (Figure 5A, right panel, red discontinuous arrows), suggesting that K⁺ ions could pass more efficiently through the mutant channel. Moreover, we saw relevant divergences in charge distribution for each channel, Kir2.1^{E299V} subunits being the most polarized and conducting, contributing to the gain-of-function (Figure 5B).

3.7 Polyamines fail to block Kir2.1 channels containing the E299V isoform

E299 is one of the cytoplasmic residues that interact with polyamines to confer strong inward rectification.^{54,55} To determine how the

E299V mutant modifies I_{K1} rectification, we conducted molecular docking experiments that included the three principal polyamines (putrescine, spermine, and spermidine) along with Kir2.1^{WT} and Kir2.1^{WT}-Kir2.1^{E299V}. All three polyamines penetrate and block Kir2.1^{WT} channels, but they fail to penetrate the cytoplasmic pore of the Kir2.1^{WT}-Kir2.1^{E299V} heterotetramer (Figure 5C and Supplementary material online, Figure S12). Therefore, the channel remains open at voltages at which it should be closed (voltages positive to -80 mV, Figure 4). Notably, the respective electro-potential data show how the docking of polyamines changes the charge distribution significantly from one Kir2.1 conformation to the other. These data also show how the polyamine is far from reaching its binding site at the heterotetrameric Kir2.1^{WT}-Kir2.1^{E299V}, leaving the channel more polarized and presumably allowing ions to pass through (Figure 5C). Altogether, these models help us understand the lack of rectification of mutant Kir2.1^{E299V} channels.

To translate these *in-silico* results to procedures in a realistic environment, we conducted inside-out patch-clamp experiments in Kir2.1^{WT} and Kir2.1^{E299V} ventricular cardiomyocytes, exposing the cytoplasmic side of the channels to different concentrations of spermine. We saw that the spermine concentration needed to block 50% of channels containing Kir2.1^{E299V} subunits was higher than for Kir2.1^{WT} homotetramers (Figure 5D). Therefore, the sensitivity of the mutant channels to the polyamine was significantly lower than WT.

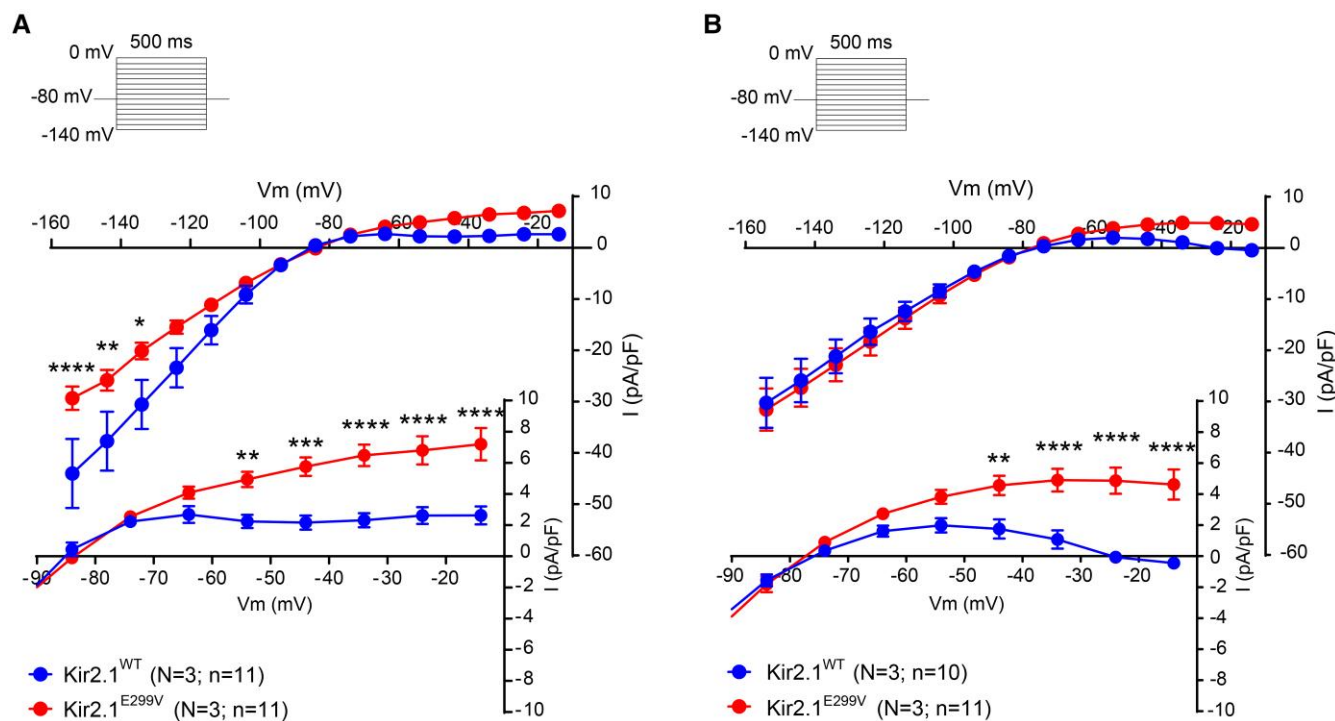


Figure 4 Kir2.1^{E299V} increases outward I_{K1} in both atria and ventricle, but reduces the slope conductance only in the atria. **A**, Atrial cardiomyocytes. Current/voltage (IV) relationships for Kir2.1^{WT} ($N = 3$, $n = 11$) and Kir2.1^{E299V} ($N = 3$; $n = 11$). Note the lack of inward-going rectification with increased outward I_{K1} at voltages positive to -60 mV (7.19 ± 1.04 pA/pF in E299V vs. 2.62 ± 0.57 pA/pF in WT, results at -14 mV; **** $P < 0.0001$) and loss of inward current at voltages negative to -120 mV (*** $P < 0.001$, ** $P < 0.01$, * $P < 0.05$ from -135 mV to -160 mV). **B**, Ventricular cardiomyocytes. I_{K1} IV relationships for both experimental groups Kir2.1^{WT} ($N = 3$, $n = 10$) and Kir2.1^{E299V} ($N = 3$; $n = 11$). Lack of inward-going rectification can be appreciated at voltages positive to -50 mV (4.62 ± 0.89 pA/pF in E299V vs. -0.41 ± 0.14 pA/pF in WT, results at -14 mV; **** $P < 0.0001$) without changes in inward current. Two-way ANOVA was applied for comparisons.

3.8 A different proportion of Kir2.x subunits in atria vs. ventricles explains the atrial-specific reduction in I_{K1} inward current and the arrhythmia inducibility

As shown above, the atria are clearly more susceptible to arrhythmias than the ventricles of the Kir2.1^{E299V} mouse, which correlates with different chamber-specific I_{K1} IV relations. Since both Kir2.1 and Kir2.2 isoforms contribute to I_{K1} in the heart⁵⁶ and it is known that these channels express differently in the atria vs. ventricles,^{22,56–61} we assessed whether different Kir2.x isoform proportions in the atria vs. the ventricle help explain the arrhythmogenic differences we observed. We first measured total Kir2.1 and Kir2.2 protein levels in atria vs. ventricles from mouse samples by western blot. We confirmed that Kir2.1 is highly expressed in the ventricles of both WT and mutant animals, whereas Kir2.1/Kir2.2 levels are close to 1 in mouse atria (Figure 6A and Supplementary material online, Figure S13). Therefore, a higher proportion of Kir2.1-Kir2.2 heterotetramers should be conducting I_{K1} in atria compared with ventricles, which possibly explained the chamber-specific differences in the pro-arrhythmic effects of the Kir2.1^{E299V} mutant channels.

To evaluate the above hypothesis, we transfected HEK-293 T cells with non-viral piggy-bac vectors encoding the designed dimers Kir2.1^{WT}-Kir2.2^{WT} and Kir2.1^{E299V}-Kir2.2^{WT} as fusion proteins. As shown in Figure 6B, cells transfected with Kir2.1^{E299V}-Kir2.2^{WT} reproduced the reduced I_{K1} inward component of atrial Kir2.1^{E299V} cardiomyocytes (see Figure 4A). Cells expressing Kir2.1^{E299V}-Kir2.2^{WT} channels had a reduced slope conductance at voltages negative to -60 mV for these specific

experimental conditions (30 mM KCl and 110 mM NaCl in the external solution to promote I_{K1} density, shifting the reversal potential from -80 to -30 mV). To assess how these changes in the atria should occur structurally, we conducted additional *in-silico* modelling of Kir2.2 heterotetramers. Mutant channels containing Kir2.1^{E299V}-Kir2.2^{WT} subunits had a reduced pore diameter and modifications in their polarity (see Supplementary material online, Figure 14A). In addition, unlike the Kir2.2^{WT} homotetramers, the Kir2.1^{E299V}-Kir2.2^{WT} heterotetramers were unable to bind polyamines or rectify properly (see Supplementary material online, Figure 14B). Moreover, analysing specifically the values, in the absence of polyamines, the pore diameter of Kir2.1^{E299V}-Kir2.2^{WT} was smaller than Kir2.1^{E299V}-Kir2.1^{WT} channels (2.4\AA vs. 4.87\AA in the extracellular pore, and 0.49\AA vs. 1.62\AA in the cytoplasmic pore, respectively) (Figure 6C). Altogether, these data suggest that the reduced pore diameter of mutant Kir2.1^{E299V}-Kir2.2^{WT} channels in atria led to relatively lower atrial than ventricular I_{K1} conductance and may underlie, at least in part, the greater arrhythmogenic potential of the atria of E299V animals.

3.9 The Kir2.1^{E299V} mutation increases ventricular excitability by modifying $Na_v1.5$ function

The ECG of the SQTS3 mouse model showed substantial abbreviation in the PR interval and a slight shortening of the QRS complex, suggesting the possibility of accelerated AV and intraventricular conduction, respectively. This might be due to sodium inward current (I_{Na}) modification induced by the Kir2.1^{E299V} mutation.^{21,34} In an additional group of experiments,

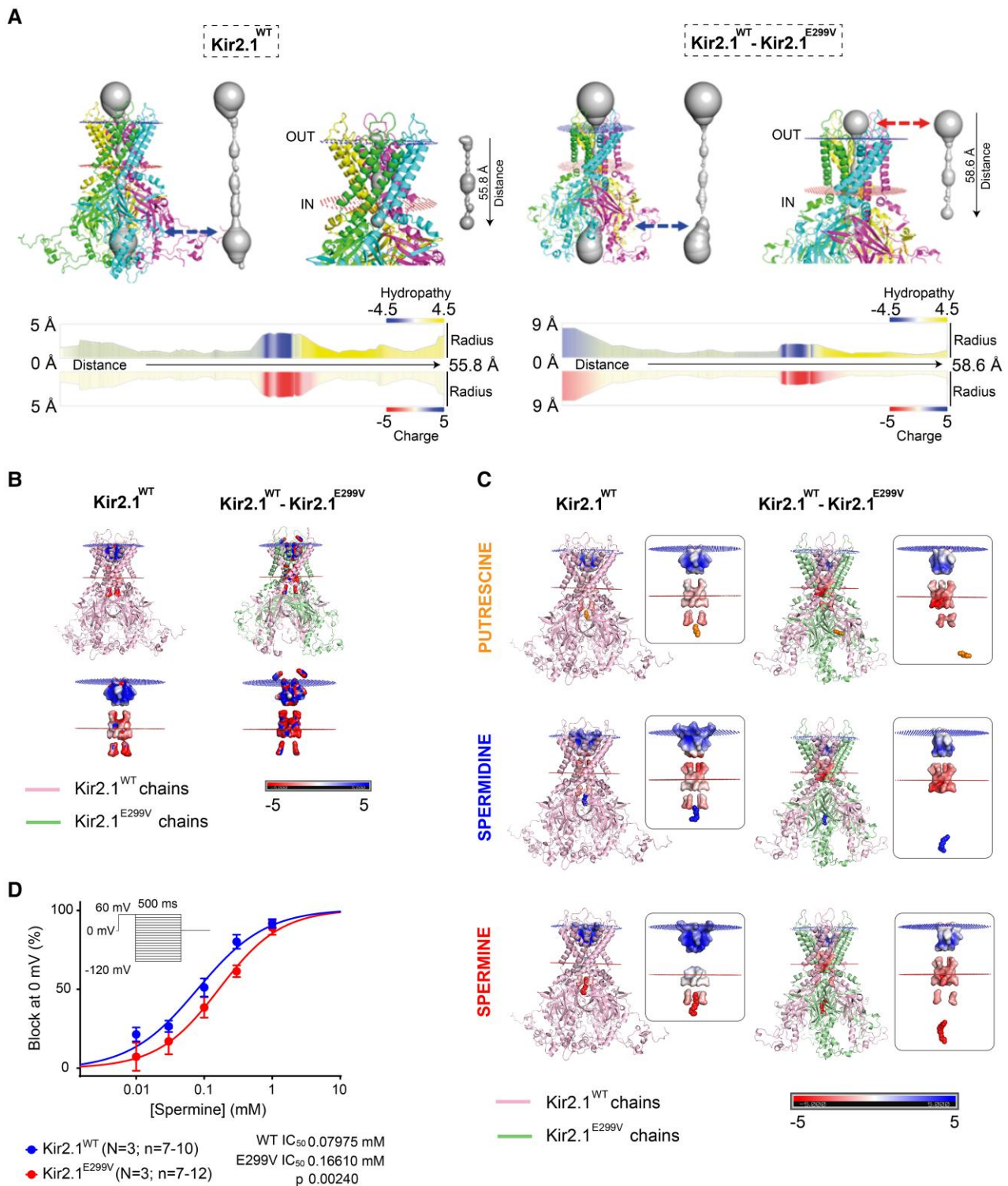


Figure 5 Polyamines fail to block Kir2.1^{E299V} channels. **A**, Top, *In-silico* models of tetrameric structure and pore conformation of Kir2.1^{WT} and Kir2.1^{WT}-Kir2.1^{E299V}. Bottom, Hydropathy, and charge maps along the extension of the pore. The cytoplasmic Kir2.1^{WT}-Kir2.1^{E299V} pore diameter is represented at the bottom of the panel and is appreciably modified by rearrangement of the side chains of residues lining the pore (dashed arrows). In contrast, the extracellular Kir2.1^{WT}-Kir2.1^{E299V} pore region undergoes significant expansion and becomes more hydrophilic (right, dashed arrows and shadows). Note the different scales in both bottom panels. **B**, Positive and negative charges distribution analysis of Kir2.1^{WT} vs. Kir2.1^{WT}-Kir2.1^{E299V}. **C**, Interaction of Kir2.1 with polyamines (putrescine, spermidine, and spermine). **D**, Spermine concentration-response curves in inside-out patch-clamp experiments (IC_{50} 0.07975 mM and 0.1661 mM for Kir2.1^{WT} and Kir2.1^{E299V}, respectively) (** P = 0.0024; N = 3, n = 7–12). P value obtained after non-linear fit analysis for comparing IC_{50} .

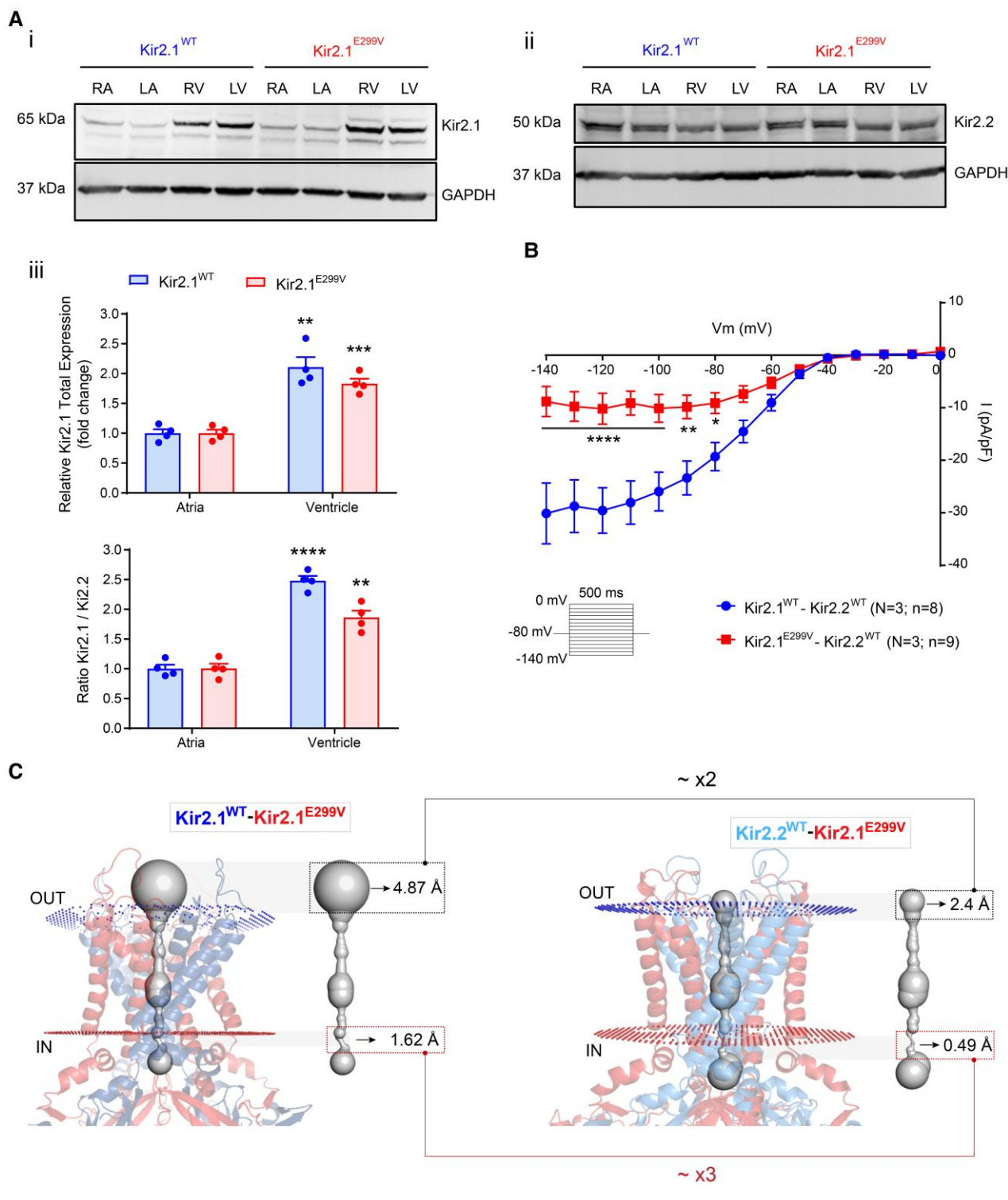


Figure 6 Abundance of Kir2.2 reduces the slope conductance of the inward I_{K1} in atrial Kir2.1^{E299V} channels. **A**, Western blots for Kir2.1 and Kir2.2 protein levels in atrial and ventricular tissue samples from mice comparing the Kir2.1 (i) and Kir2.2 (ii) expression levels. (iii) Quantification of total Kir2.1 protein levels (top) and Kir.1/Kir2.2 ratio (bottom) in atria vs. ventricles from Kir2.1^{WT} and Kir2.1^{E299V} animals (** $P < 0.01$, *** $P < 0.001$ and **** $P < 0.0001$; duplicate experiments in $N = 4$ animals per condition; Glyceraldehyde-3-phosphate dehydrogenase (GAPDH) was used as loading control for all comparisons). **B**, IV relationship of I_{K1} in HEK-293 cells transfected with dimers expressing Kir2.1^{WT}-Kir2.2^{WT} or Kir2.1^{E299V}-Kir2.2^{WT} ($N = 3$ independent transfections; $n = 8-9$ cells per condition; $P < 0.05$ for voltages negative to -80 mV). We used a modified external solution (30 mM KCl and 110 mM NaCl) to promote the I_{K1} current, shifting the reversal potential towards more positive voltages (from -80 to -30 mV). **C**, *In-silico* simulations of Kir2.1^{WT}-Kir2.1^{E299V} compared to Kir2.1^{E299V}-Kir2.2^{WT} (2.4 Å vs. 4.87 Å in the extracellular pore of Kir2.1^{E299V}-Kir2.2^{WT} and Kir2.1^{WT}-Kir2.2^{WT}, respectively; 0.49 Å vs. 1.62 Å in the cytoplasmic pore for Kir2.1^{E299V}-Kir2.2^{WT} and Kir2.1^{WT}-Kir2.1^{E299V}, respectively). We applied Welch's *t*-test and two-way ANOVA for comparisons.

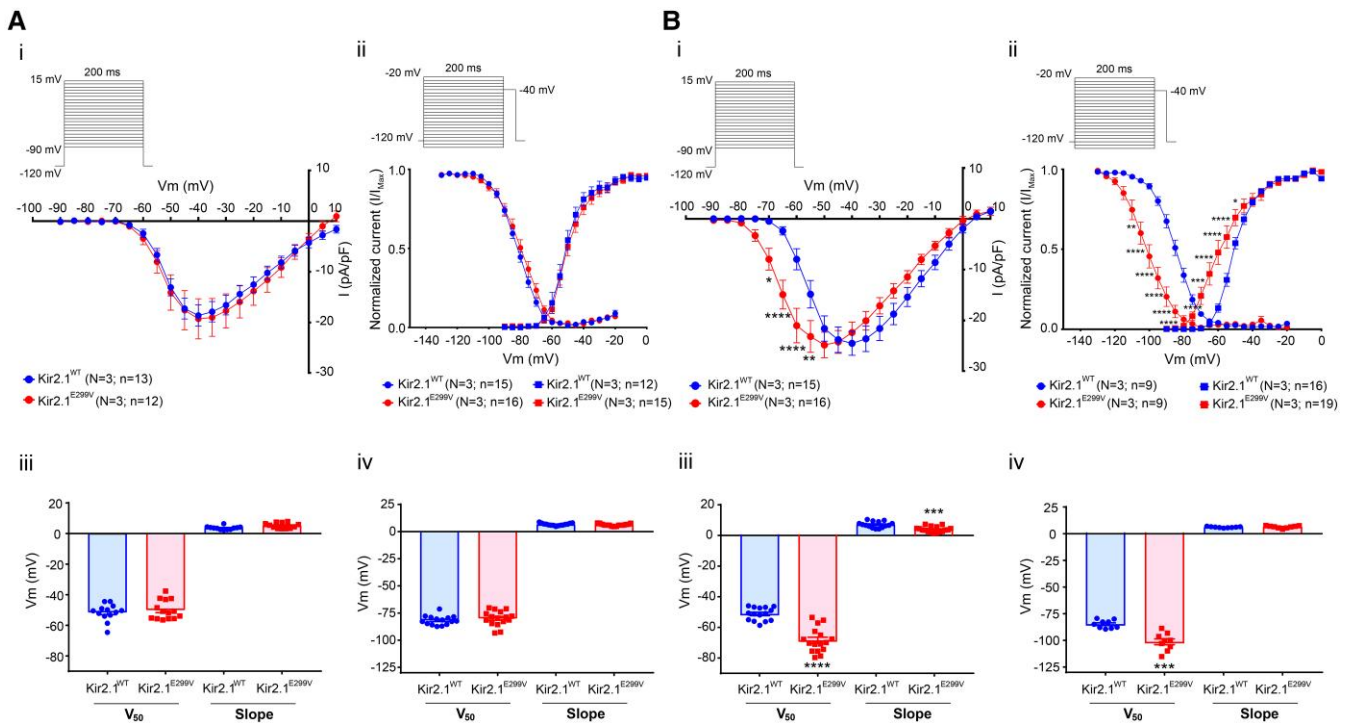


Figure 7 Kir2.1^{E299V} modifies sodium current properties in ventricular but not atrial cardiomyocytes. Electrophysiological characterization of sodium currents (I_{Na}) from Kir2.1^{WT} and Kir2.1^{E299V} isolated cardiomyocytes. **A**, Atrial cardiomyocytes. Kir2.1^{WT} ($N = 3$, $n = 13$ – 15) and Kir2.1^{E299V} ($N = 3$, $n = 12$ – 16). **B**, Ventricular cardiomyocytes. Kir2.1^{WT} ($N = 3$, $n = 9$ – 16) and Kir2.1^{E299V} ($N = 3$, $n = 9$ – 19). (i) Different panels in both regions show the I_{Na} IV relationships ($***P < 0.001$, $**P < 0.01$, and $*P < 0.05$ for voltages from -70 to -55 mV when comparing WT and mutant ventricular cardiomyocytes). (ii) I_{Na} inactivation and activation curves. Note the shift to negative voltages in the I_{Na} inactivation and activation curves of Kir2.1^{E299V} ventricular cardiomyocytes ($****P < 0.0001$, $***P < 0.001$, $**P < 0.01$, and $*P < 0.05$). The activation ($****P < 0.0001$ and $***P < 0.001$ when comparing WT and mutant ventricular cardiomyocytes) (iii) and inactivation ($***P > 0.001$ also in WT vs. mutant ventricular myocytes) (iv) parameters (V_{50} and slope) are also indicated. Two-way ANOVA and Mann-Whitney test were applied for comparisons.

we measured I_{Na} in atrial and ventricular cardiomyocytes. In **Figure 7A** superimposed IV relations (Ai), and activation and inactivation curves (Aii) from Kir2.1^{WT} and Kir2.1^{E299V} atrial cardiomyocytes showed that the mutation did not modify either I_{Na} density or its biophysical properties (Aiii and Aiv). In **Figure 7B**, the results were completely different for ventricular cardiomyocytes, where the mutation led to a large and significant shift of I_{Na} peak density to the left (Bi) and an equal shift of both activation and inactivation to negative voltages (**Figure 7Bii-iv**).

To study if the above effects resulted in accelerated conduction in mutant ventricles, we performed optical mapping experiments (see **Supplementary material online, Figure S15**). Mean ventricular CV was higher in Kir2.1^{E299V} than Kir2.1^{WT} hearts. Ventricular CV in Kir2.1^{E299V} was also higher than both left and right atria from Kir2.1^{WT} and Kir2.1^{E299V} hearts, which were similar to WT ventricles. These data provide proof that by increasing excitability in ventricular cardiomyocytes, the Kir2.1^{E299V} mutation also increases CV, which likely protects the ventricles against the initiation and maintenance of arrhythmias.

Further analysis of Kir2.1- $Na_v1.5$ channelosome-related proteins^{20,34} confirmed similar expression levels and distribution patterns of Kir2.1, $Na_v1.5$, $\alpha1$ -Syntrophin, and SAP97 between groups (see **Supplementary material online, Figures S16 and S17**), suggesting that chamber-specific changes in the biophysical properties of I_{Na} were independent of channelosome trafficking or scaffolding, at least at the confocal resolution limit.

To investigate more about the mechanisms underlying the differential I_{Na} changes in ventricular vs. atrial Kir2.1^{E299V} cardiomyocytes, we used HEK-293 T cells stably expressing $Na_v1.5$ (HEK- $Na_v1.5$ cells).³⁵ We

transfected Kir2.1^{WT} and Kir2.1^{E299V} to simulate a mutant heterozygous condition in HEK- $Na_v1.5$ cells. We saw no differences in I_{Na} density between WT vs. mutant conditions as we had in atrial cardiomyocytes (see **Supplementary material online, Figure S18**). In addition to the interactors mentioned above, β subunits play important roles in the regulation of $Na_v1.5$ trafficking and function.^{35,62–66} $Na_v\beta2$ and $Na_v\beta4$ are $Na_v1.5$ regulatory subunits differently expressed in atria vs. ventricles, having a higher presence in murine ventricles.^{64,67,68} Hence, in HEK- $Na_v1.5$ cells expressing Kir2.1^{WT} and Kir2.1^{WT/E299V}, we transfected β subunits individually and in combination. The most promising results were obtained in cells expressing Kir2.1^{WT/E299V} + $Na_v\beta4$. While we did not observe any changes in inactivation, we saw a slight shift of activation to negative voltages and an increase in I_{Na} density (see **Supplementary material online, Figure S18**). Surely other interactors are likely involved, but $Na_v\beta4$ appears to be contributing in some way to the Kir2.1^{E299V}-mediated modification of $Na_v1.5$ properties in the ventricles where this subunit is highly expressed.⁶⁸

3.10 The Kir2.1^{E299V} mutation increases I_{Na} density in Purkinje cardiomyocytes

The slight abbreviation in the QRS complex duration in Kir2.1^{E299V} mice suggested a confirmed increase in the ventricular CV. Then, we wanted to know the reason for the PR interval shortening in mutant animals. We infected transgenic Cx40^{GFP} with AAV-Kir2.1^{WT} and AAV-Kir2.1^{E299V} to localize and isolate infected Purkinje cardiomyocytes and determine changes in I_{K1}

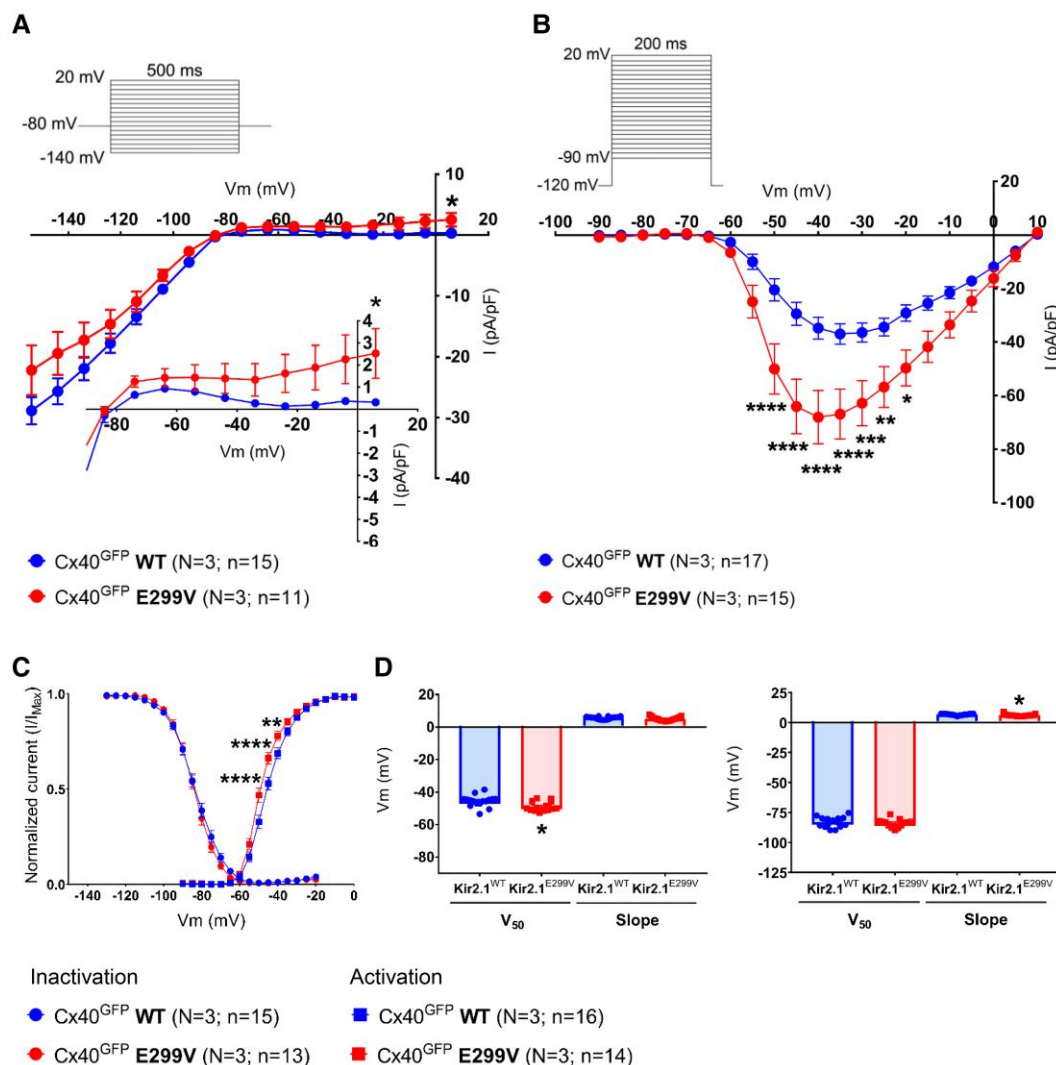


Figure 8 Kir2.1^{E299V} increases I_{Na} density in cardiac Purkinje cardiomyocytes. A, I_{K1} IV relationships for Cx40^{GFP} AAV-Kir2.1^{WT} (N = 3, n = 15) and Cx40^{GFP} AAV-Kir2.1^{E299V} (N = 3, n = 11) Purkinje cells (*P = 0.0163 at +6 mV). B, Superimposed I_{Na} IV relationships (N = 3 and n = 15–17; ****P < 0.0001, ***P < 0.001, **P < 0.01, and *P < 0.05 when indicated). C, Sodium activation and inactivation curves (N = 3, n = 13–16; ****P < 0.0001 and **P < 0.01). D, Graphs show sodium activation (left panel) and inactivation (right panel) parameters (V₅₀ and slope) (N = 3; n = 13–16, *P < 0.05). Two-way ANOVA (IV and sodium activation/inactivation curves) and Mann–Whitney test (activation/inactivation parameters) applied for comparisons.

and I_{Na}.^{33,69–72} I_{K1} recordings showed a small but significant reduction of inward-going rectification in Cx40^{GFP}-Kir2.1^{E299V} compared to control Cx40^{GFP}-Kir2.1^{WT} cells (Figure 8A). However, a more remarkable difference occurred at the cardiac sodium current level: Cx40^{GFP}-Kir2.1^{E299V} cells manifested a significantly higher I_{Na} density than Cx40^{GFP}-Kir2.1^{WT} cells, and a shift of I_{Na} activation to negative voltages (Figure 8B–D). Together, these results clearly explain the shortening of the PR interval and the slightly abbreviated QRS complex of mutant mice. They contribute to a higher CV conferring protection against ventricular arrhythmias in Kir2.1^{E299V} mice, and explaining their chamber-specific inducibility.

4. Discussion

The most important results of this original study are as follows: (i) We have generated the first *in-vivo* model of SQT3S able to reproduce the phenotypical electrical characteristics of a patient with the Kir2.1^{E299V} mutation.¹⁴ (ii) On ECG, the QT interval of Kir2.1^{E299V} mice was significantly

shorter than Kir2.1^{WT} mice. (iii) Arrhythmia inducibility was greater in the atria than in the ventricles of Kir2.1^{E299V} mice. (iv) Both atrial and ventricular Kir2.1^{E299V} cardiomyocytes generated extremely abbreviated APs due to lack of inward-going rectification. (v) There were significant chamber-specific effects of the Kir2.1^{E299V} mutation at the ion channel level: while in Kir2.1^{E299V} atrial cardiomyocytes I_{K1} presented a reduced slope conductance, in ventricular cardiomyocytes the mutation increased cell excitability by shifting I_{Na} activation and steady-state inactivation in the hyperpolarizing direction, which protected the ventricles against arrhythmia induction. In addition, in the cardiac conduction system cells, the mutation caused a higher I_{Na} density contributing to increase the CV. Therefore, in the ventricles, the Kir2.1^{E299V} mutation reduces Kir2.1 current rectification to shorten the APD and increases excitability by modifying Na_v1.5 function. (vi) In atrial cardiomyocytes, while the mutation increased the outward I_{K1} at positive voltages, a greater proportion of Kir2.1^{E299V}-Kir2.2^{WT} channels impaired polyamine block in the presence of a reduced pore diameter. Altogether, the results provide novel functional interactions between Kir2.1 and Na_v1.5 channels and insight into the

mechanism underlying greater atrial than ventricular arrhythmogenesis in the mouse model and a patient with SQT3S due to the Kir2.1^{E299V} mutation.

We used AAV9 technology²⁶ to generate the first SQT3S mouse model with gene constructs containing Kir2.1^{E299V} vs. the Kir2.1^{WT} version as control. The cardiac mechanisms are too complex to investigate them in heterologous expression systems, and here we provide an *in-vivo* model that changes the landscape for the study of hereditary arrhythmias associated with SQT3S. Introduction of exogenous human Kir2.1^{E299V} in mice expressing the murine Kir2.1^{WT} endogenously reproduces a heterozygous condition where the dominant negative effect of the mutation mimics the patient's genetic environment in the heart. Importantly, infection using the human WT or mutant Kir2.1 sequences did not alter the endogenous expression of Kir2.x subtypes or caused Kir2.1 overexpression in the cardiac tissue.

Mutant mice presented significant QT abbreviation and increased susceptibility to arrhythmias. Programmed electrical stimulation (PES) in the right atria, His bundle or RV of Kir2.1^{WT} and Kir2.1^{E299V} groups demonstrated that, by far, the largest proportion of mutant mice responded with supraventricular arrhythmias like AF. Also, the longest-lasting events were recorded in the atria. At the ionic level, Kir2.1^{E299V} ventricular cardiomyocytes revealed a gain-of-function in the outward I_{K1} due to a lack of inward-going rectification. This behaviour was similar in mutant atrial cardiomyocytes, which, unlike the ventricles, also had reduced I_{K1} at potentials negative to -80 mV. *In-silico* structural modelling and inside-out patch-clamp experiments confirmed the lack of rectification in Kir2.1^{E299V} cardiomyocytes underlying the gain-of-function. As glutamic acid was replaced by valine, the mutation induced a loss of negative charges in the channel pore. Consequently, positively charged polyamines failed to penetrate sufficiently to block mutant Kir2.1^{E299V} channels.

There is increasing evidence that channels function as part of macromolecular complexes and interact with other proteins, including ion channels.^{21–25,34,36,73,74} Evidence also indicates that mutations in ionic channels or in their regulatory subunits cause modifications in the functional, structural, or kinetic properties of many other interactors.^{23,24,34} Some of them are important in maintaining excitability and excitation–contraction coupling, so punctual genetic alterations in apparently unrelated proteins provoke unexpected changes in other cell functions. Thus, we should not treat channelopathies as monogenic diseases, since even though they may be caused by specific mutations in one gene, a given mutation also affects the products of other genes. Such a premise was borne out in the *in-vivo* SQT3S model, which allowed the discovery that the Kir2.1^{E299V} mutation modified the biophysical properties of the I_{Na} in ventricular cardiomyocytes and its density in cardiac Purkinje cells. In mutant ventricular cardiomyocytes, Nav1.5 activates at more negative voltages than WT and its inactivation is also left-shifted, which likely contributed to increasing I_{Na} availability at potentials between -80 and -60 mV.

The speed of excitation of a cardiomyocyte in response to an external stimulus is determined by the rate of approach to threshold (foot potential) and the maximum rate of depolarization (dV/dt_{max}) during phase 0 of the AP (see [Supplementary material online, Figure S19A](#)). The foot potential depends on the balance between the magnitude of inward current provided by the stimulus, the time needed to charge the membrane capacitance and the amount of outward I_{K1} opposing the depolarization. Once threshold has been reached, dV/dt_{max} will depend on the number of sodium channels available for excitation.⁷⁵ Similarly, the velocity of impulse propagation in the cardiac syncytium will depend on the amount of charge carried by the AP of a given cardiomyocyte to excite downstream neighbours, the time needed to charge their membrane capacitance, the amount of outward I_{K1} opposing depolarization and the availability of sodium channels for excitation.⁷⁶ Thus, to determine why CV increased in the mutant ventricles with respect to WT, in cardiomyocytes we compared the amount of current needed to reach threshold as the relation between sodium channel availability and the charge needed for excitation, normalized by the access resistance (see [Supplementary material online, Figure S19B](#)). Therefore, despite the absence of dV/dt_{max} change, the more negative threshold potential and lower current needed for excitation likely enabled

for a shorter foot of the conducted AP, accelerating conduction in the mutant ventricles, which accounted for the slightly shorter QRS interval. On the other hand, the increased I_{Na} density in the mutant Purkinje fiber network was likely responsible for the shortening of the PR interval. Hence, unexpectedly, the same mutation differentially affected each of the cardiac chamber and cell type, which explains the atrial arrhythmia predisposition and absence of ventricular arrhythmias in the mouse and the patient with the Kir2.1^{E299V} mutation. Most likely, specific Kir2.1 interactors in each of the cardiac regions modify the electrical properties differently, which should explain the dissimilar outcomes with the same mutation.

Kir2.1 and Nav1.5 traffic together from the sarcoplasmic reticulum and they interact with multiple proteins capable of modifying their targeting and distribution.^{21–25,34,36,73,74} Proteins like SAP97 and α 1-Syntrophin act as scaffolds that keep Kir2.1 and Nav1.5 together at the membrane through their PDZ (Postsynaptic density protein, *Drosophila* disc large tumour suppressor, and Zonula occludens-1 protein) binding domains. *In-vitro* experiments have demonstrated that inhibition or absence of these interacting proteins causes alterations in both I_{K1} and I_{Na} .^{20,22,77–81} However, in ventricular cardiomyocytes expressing Kir2.1^{E299V}, we have not seen changes in the distribution or levels of either channel or their specific interactors, which rule out the above proteins as mediators of the arrhythmogenic consequences of the mutation.

Some of the Nav1.5 β subunits are known to predictably modify I_{Na} activation and inactivation^{35,62–68} in cardiac and other excitable cells, and they also interact with other channels. Hu *et al.* demonstrated that a variant in *SCN1Bb* gene encoding the β 1 subunit caused alterations in I_{Na} and I_{to} , as β 1 has functional and structural association with both Nav1.5 and $K_v4.3$.⁸² These regulatory subunits would be interacting with other apparently unrelated channels and taking part of the same macromolecular complexes. Nav1.5 β 2 and β 4 are expressed mainly in the ventricles.⁶⁸ Apparently, Nav1.5 β 2 alone does not have effects on the kinetic properties of Nav1.5,³⁵ but Nav1.5 β 4 expression would be able to change I_{Na} biophysical parameters.⁶² However, transfection with Kir2.1^{E299V} along with β 4 in the HEK-Nav1.5 cell line failed to reproduce the results seen in mutant ventricular cardiomyocytes (see [Supplementary material online, Figure S18](#)). The question remains why the Kir2.1^{E299V} mutation leads to such an unexpected gain-of-function modification in Nav1.5 so specifically in ventricular but not atrial cardiomyocytes. Answering this question will require exploration of yet unidentified but possible Kir2.1 interactions with Nav1.5 partner proteins.

The atria have certain characteristics that may contribute to arrhythmogenesis in light of APD shortening induced by I_{K1} gain-of-function. The complex anatomy of the atria is potentially arrhythmogenic due in part to the highly intricate arrangement of the endocardial pectinate muscles, which may facilitate both inducibility and maintenance of AF.⁸³ Computational and experimental studies have demonstrated that the pectinate muscles contribute stabilizing re-entry and fibrillatory conduction.⁸⁴ Moreover, the spatially heterogeneous ion channel distribution and electrical properties throughout both atria also make them particularly susceptible to arrhythmias due to I_{K1} gain-of-function,⁸⁵ even in the absence of other electrophysiological alterations.

Panama *et al.* showed that both Kir2.x expression and I_{K1} properties are spatially heterogeneous in the mouse heart.⁵⁹ Gaborit *et al.* demonstrated that the ventricles express higher levels of Kir2.1, but the expression profile of Kir2.2 was the same in both cardiac chambers.⁸⁶ Here, we confirmed that the ventricles have higher levels of Kir2.1 than the atria, a pattern that remains even in the presence of the E299V mutation ([Figure 6](#)). Seeing slightly higher levels of Kir2.2 in murine atria than ventricles, we assumed that in the atrium there is a larger number of Kir2.x channels containing Kir2.2 subunits compared with the ventricles. I_{K1} generated by dimers expressing Kir2.1^{E299V}-Kir2.2^{WT} and transfected into HEK-293 T cells was similar to atrial cardiomyocytes. In addition, heterotetrameric Kir2.1^{E299V}-Kir2.2^{WT} channels simulated *in-silico* had a reduced pore diameter that could explain their reduced conductance at voltages negative to -80 mV. We, therefore, propose that, together with the complex cardiac structure, such a low Kir2.1 pore conductivity underlies the greater atrial than ventricular arrhythmogenic potential in the Kir2.1^{E299V} mice.

The young patient in whom we discovered the Kir2.1^{E299V} mutation presented an extremely short QTc interval and AF. Such a phenotype provides validation to our results, as the mouse recapitulated the most important aspects of the patient's electrical phenotype. However, extrapolation of our results to the clinic and the patient with SQT3 should be done with extreme caution. After all, Kir2.3 is the most predominant Kir2.x subtype in the human atrium,⁸⁶ and it does not interact reciprocally with Nav1.5 channels.²² We, therefore, conducted additional *in silico* studies using Kir2.1^{E299V}-Kir2.3^{WT} heterotetramers (see [Supplementary material online, Figure S20](#)). The simulated channels had defects in the pore and its polarity, and were unable to bind polyamines, indicating they would not rectify either in human atrial cardiomyocytes. Therefore, even without any modifications in the voltage dependence and biophysical properties of Nav1.5, the absence of I_{K1} rectification and reduced pore conductance caused by the Kir2.1^{E299V} mutation in atrial cardiomyocytes would be sufficient to underlie the initiation and maintenance of AF in the heterogeneous atria of a SQT3 patient.

Additionally, our results establish the molecular basis of SQT3 and open new strategic lines for the development of drugs based on the polyamines' skeleton. These positively charged molecules present a high capacity for blocking Kir2.1 and could be chemically modified for reducing the hyperfunctionality of Kir2.1^{E299V} mutant channels. These new therapies may help to preventing life-threatening arrhythmias and SCD in SQT3 and possibly other diseases.

In conclusion, this work contributes to unravel the arrhythmogenic consequences of the gain-of-function mutation Kir2.1^{E299V} causing SQT3. Knowing the molecular and electrical environment that triggers lethal arrhythmias in patients suffering from this syndrome may lead to develop diagnostic tools and new therapeutic strategies to reduce their morbidity and mortality. Moreover, unravelling the molecular mechanisms underlying rare and lethal syndromes, such as SQT3, contributes to increase knowledge that can be applied to the management of other more prevalent cardiac diseases.

4.1 Limitations

We have used mice to investigate arrhythmogenic mechanisms in SQT3, but we are well aware of the potential limitations of this animal model to study a human disease. Heart rate and repolarization features between mice and humans are different, as they are governed by different sets of potassium currents, a fact that alters the AP and QT interval durations. For example, mice do not present I_{Kr} or I_{Ks}, the rapid and slow delayed rectifier currents. This sense, while chloroquine and flecainide are known to inhibit not only I_{K1}, but I_{Kr} as well, the latter effect would not be reflected in mouse QT data. Structurally, there are also remarkable differences between the murine and human hearts, such as the heart size. Therefore, results about specific mechanisms of arrhythmia in the mice should not be extrapolated directly to the clinic, and more studies using appropriate pre-clinical models would be needed to ensure rigorous translation of our results to the human patient. Moreover, regarding the AAVs, although AAV vectors delivered to the heart show a high rate of infection (over 95%) and genetic load (over 60% of the cardiomyocytes have between one and three copies of the transgene), this system always generates a mosaic cellular distribution of Kir2.1^{WT} and Kir2.1^{E299V} expression in the heart. Yet, despite the above limitations, we stand by our results, which provide novel insights into the mechanisms of differential chamber-specific electrical remodelling underlying atrial arrhythmogenesis and ventricular protection in a mouse model of SQT3.

Supplementary material

Supplementary material is available at *Cardiovascular Research* online.

Author contribution

A.I.M.M., A.M., F.M.C. J.A.B., and J.J. co-designed the experiments; A.M. is corresponding author for cellular electrophysiology; and F.M.C. is

corresponding author for the mouse models *in-vivo* characterization; A.I.M.M., A.M., and F.M.C. performed most cellular, *ex-vivo* and *in-vivo* experiments; L.K.G. carried out the optical mapping experiments; L.K.G. and F.M. were in charge of *in-silico* modelling and molecular docking studies; A.G.G., F.M.C., and J.A.B. designed the vectors and generated the AAV9-dependent mouse models; I.M.C., F.B.J., P.S.P., M.L.V.P., and J.M.R. provided technical support, discussions, and revisions; A.I.M.M. and J.J. co-wrote the manuscript; J.A.B. and J.J. conceived the study, and provided supervision, funding, and revisions; all authors discussed the results and commented on and approved the manuscript.

Acknowledgements

We thank the CNIC Viral Vectors Unit for producing the AAV9 used in this article. We thank the CNIC Bioinformatics Unit for generating the *in-silico* simulations and helping in their discussion. We thank Carmen Valenzuela's laboratory and Hugues Abriel's laboratory members for their help with HEK-Nav1.5 cells and Navβ subunits plasmids, respectively. The confocal experiments were carried out in the CNIC Microscopy and Dynamic Imaging Unit—ICTS-ReDib with funding from MCIN/AEI/10.13039/501100011033 and FEDER 'Una manera de hacer Europa' (#ICTS-2018-04-CNIC-16).

Conflict of interest: none declared.

Funding

This work was supported by 'La Caixa' Foundation [project code LCF/PR/HR19/52160013]; grant PI20/01220 of the public call 'Proyectos de Investigación en Salud 2020' [PI-FIS-2020] funded by Instituto de Salud Carlos III (ISCIII); MCIU grant BFU2016-75144-R and PID2020-116935RB-I00, and co-funded by Fondo Europeo de Desarrollo Regional (FEDER); and Fundació La Marató de TV3 [736/C/2020]. We also receive support from the European Union's 'Horizon 2020 Research and Innovation Framework Programme' [grant agreement GA-965286]; the Dynamic Microscopy and Imaging Unit—ICTS-ReDib Grant ICTS-2018-04-CNIC-16 funded by MCIN/AEI/10.13039/501100011033 and ERDF 'A way of making Europe'; project EQC2018-005070-P funded by MCIN/AEI/10.13039/501100011033 and FEDER 'Una manera de hacer Europa'. CNIC is supported by the Instituto de Salud Carlos III (ISCIII), the Ministerio de Ciencia e Innovación (MCIN) and the Pro CNIC Foundation, and is a Severo Ochoa Center of Excellence [grant CEX2020-001041-S funded by MCIN/AEI/10.13039/501100011033].

A.I.M.M. holds a FPU contract [FPU20/01569] from Ministerio de Universidades. L.K.G. holds a FPI contract [PRE2018-083530], Ministerio de Economía y Competitividad de España co-funded by Fondo Social Europeo 'El Fondo Social Europeo invierte en tu futuro', attached to Project SEV-2015-0505-18-2. I.M.C. holds a PFIS contract [FI21/00243] funded by Instituto de Salud Carlos III and Fondo Social Europeo Plus (FSE+), 'co-funded by the European Union'. M.L.V.P. held contract PEJD-2019-PRE/BMD-15982 funded by Consejería de Educación e Investigación de la Comunidad de Madrid 'El FSE invierte en tu futuro'.

Data availability

The data underlying this article are available in the article and in its online supplementary material. Additional data will be shared on request to the corresponding authors.

References

- Gaita F, Giustetto C, Bianchi F, Wolpert C, Schimpf R, Riccardi R, Grossi S, Richiardi E, Borggrefe M. Short QT syndrome: a familial cause of sudden death. *Circulation* 2003;**108**: 965–970.
- Giustetto C, Di Monte F, Wolpert C, Borggrefe M, Schimpf R, Sbragia P, Leone G, Maury P, Anttonen O, Haissaguerre M, Gaita F. Short QT syndrome: clinical findings and diagnostic-therapeutic implications. *Eur Heart J* 2006;**27**:2440–2447.
- Gussak I, Brugada P, Brugada J, Wright RS, Kopecky SL, Chaitman BR, Bjerregaard P. Idiopathic short QT interval: a new clinical syndrome? *Cardiology* 2000;**94**:99–102.

4. Fernández-Falgueras A, Sarquella-Brugada G, Brugada J, Brugada R, Campuzano O. Cardiac channelopathies and sudden death: recent clinical and genetic advances. *Biology (Basel)* 2017; **6**:7.
5. Giustetto C, Schimpf R, Mazzanti A, Scrocco C, Maury P, Anttonen O, Probst V, Blanc JJ, Sbragia P, Dalmaso P, Borggrefe M, Gaita F. Long-term follow-up of patients with short QT syndrome. *J Am Coll Cardiol* 2011; **58**:587–595.
6. Mazzanti A, Kanthan A, Monteforte N, Memmi M, Bloise R, Novelli V, Miceli C, O'Rourke S, Borio G, Zienciu-Krajka A, Curcio A, Surducian AE, Colombo M, Napolitano C, Priori SG. Novel insight into the natural history of short QT syndrome. *J Am Coll Cardiol* 2014; **63**:1300–1308.
7. Campuzano O, Fernandez-Falgueras A, Lemus X, Sarquella-Brugada G, Cesar S, Coll M, Mates J, Arbelo E, Jorda P, Perez-Serra A, Del Olmo B, Ferrer-Costa C, Iglesias A, Fiol V, Puigmule M, Lopez L, Pico F, Brugada J, Brugada R. Short QT syndrome: a comprehensive genetic interpretation and clinical translation of rare variants. *J Clin Med* 2019; **8**:1035.
8. Walsh R, Adler A, Amin AS, Abiusi E, Care M, Bikker H, Amenta S, Feilolter H, Nannenber EA, Mazarrotto F, Trevisan V, Garcia J, Hershberger RE, Perez MV, Sturm AC, Ware JS, Zareba W, Novelli V, Wilde AAM, Gollub MH. Evaluation of gene validity for CPVT and short QT syndrome in sudden arrhythmic death. *Eur Heart J* 2022; **43**:1500–1510.
9. Thorsen K, Dam VS, Kjaer-Sorensen K, Pedersen LN, Skeberdis VA, Jurevicius J, Treinys R, Petersen I, Nielsen MS, Oxvig C, Morth JP, Matchkov VV, Aalkjaer C, Bundgaard H, Jensen HK. Loss-of-activity-mutation in the cardiac chloride-bicarbonate exchanger AE3 causes short QT syndrome. *Nat Commun* 2017; **8**:1696.
10. Hattori T, Makiyama T, Akao M, Ehara E, Ohno S, Iguchi M, Nishio Y, Sasaki K, Itoh H, Yokode M, Kita T, Horie M, Kimura T. A novel gain-of-function KCNJ2 mutation associated with short-QT syndrome impairs inward rectification of Kir2.1 currents. *Cardiovasc Res* 2012; **93**:666–673.
11. Priori SG, Pandit SV, Rivolta I, Berenfeld O, Ronchetti E, Dharmoon A, Napolitano C, Anumonwo J, di Barletta MR, Gudappakkam S, Bosi G, Stramba-Badiale M, Jalife J. A novel form of short QT syndrome (SQT3) is caused by a mutation in the KCNJ2 gene. *Circ Res* 2005; **96**:800–807.
12. Nichols CG, Lopatin AN. Inward rectifier potassium channels. *Annu Rev Physiol* 1997; **59**:171–191.
13. Hibino H, Inanobe A, Furutani K, Murakami S, Findlay I, Kurachi Y. Inwardly rectifying potassium channels: their structure, function, and physiological roles. *Physiol Rev* 2010; **90**:291–366.
14. Deo M, Ruan Y, Pandit SV, Shah K, Berenfeld O, Blaufox A, Cerrone M, Noujaim SF, Denegri M, Jalife J, Priori SG. KCNJ2 mutation in short QT syndrome 3 results in atrial fibrillation and ventricular proarrhythmia. *Proc Natl Acad Sci U S A* 2013; **110**:4291–4296.
15. Bichet D, Haass FA, Jan LY. Merging functional studies with structures of inward-rectifier K(+) channels. *Nat Rev Neurosci* 2003; **4**:957–967.
16. Lopatin AN, Makhina EN, Nichols CG. The mechanism of inward rectification of potassium channels: “long-pore plugging” by cytoplasmic polyamines. *J Gen Physiol* 1995; **106**:923–955.
17. Liu TA, Chang HK, Shieh RC. Revisiting inward rectification: K ions permeate through Kir2.1 channels during high-affinity block by spermidine. *J Gen Physiol* 2012; **139**:245–259.
18. Pegan S, Arrabit C, Zhou W, Kwiatkowski W, Collins A, Slesinger PA, Choe S. Cytoplasmic domain structures of Kir2.1 and Kir3.1 show sites for modulating gating and rectification. *Nat Neurosci* 2005; **8**:279–287.
19. Pegg AE. Functions of polyamines in mammals. *J Biol Chem* 2016; **291**:14904–14912.
20. Milstien ML, Musa H, Balbuena DP, Anumonwo JM, Auerbach DS, Fursan PB, Hou L, Hu B, Schumaker SM, Vaidyanathan R, Martens JR, Jalife J. Dynamic reciprocity of sodium and potassium channel expression in a macromolecular complex controls cardiac excitability and arrhythmia. *Proc Natl Acad Sci U S A* 2012; **109**:E2134–E2143.
21. Manuel AIM, Gutierrez LK, Pedrosa MLV, Urendez FMC, Jimenez FJB, Carrascoso IM, Perez PS, Macias A, Jalife J. Molecular stratification of arrhythmogenic mechanisms in the Andersen Tawil Syndrome. *Cardiovasc Res* 2022; **119**:919–932.
22. Matamoros M, Perez-Hernandez M, Guerrero-Serna G, Amoros I, Barana A, Nunez M, Ponce-Balbuena D, Sacristan S, Gomez R, Tamargo J, Caballero R, Jalife J, Delpon E. Nav1.5 N-terminal domain binding to alpha1-syntrophin increases membrane density of human Kir2.1, Kir2.2 and Nav1.5 channels. *Cardiovasc Res* 2016; **110**:279–290.
23. Perez-Hernandez M, Matamoros M, Alfayate S, Nieto-Marin P, Utrilla RG, Tinaquero D, de Andres R, Crespo T, Ponce-Balbuena D, Willis BC, Jimenez-Vazquez EN, Guerrero-Serna G, da Rocha AM, Campbell K, Herron TJ, Diez-Guerra FJ, Tamargo J, Jalife J, Caballero R, Delpon E. Brugada syndrome trafficking-defective Nav1.5 channels can trap cardiac Kir2.1/2.2 channels. *JCI Insight* 2018; **3**:e96291.
24. Ponce-Balbuena D, Guerrero-Serna G, Valdivia CR, Caballero R, Diez-Guerra FJ, Jimenez-Vazquez EN, Ramirez RJ, da Rocha A M, Herron TJ, Campbell KF, Willis BC, Alvarado FJ, Zarzoso M, Kaur K, Perez-Hernandez M, Matamoros M, Valdivia HH, Delpon E, Jalife J. Cardiac Kir2.1 and Nav1.5 channels traffic together to the sarcolemma to control excitability. *Circ Res* 2018; **122**:1501–1516.
25. Utrilla RG, Nieto-Marin P, Alfayate S, Tinaquero D, Matamoros M, Perez-Hernandez M, Sacristan S, Ondo L, de Andres R, Diez-Guerra FJ, Tamargo J, Delpon E, Caballero R. Kir2.1-Nav1.5 channel complexes are differently regulated than Kir2.1 and Nav1.5 channels alone. *Front Physiol* 2017; **8**:903.
26. Cruz FM, Sanz-Rosa D, Roche-Molina M, Garcia-Prieto J, Garcia-Ruiz JM, Pizarro G, Jimenez-Borreguero LJ, Torres M, Bernad A, Ruiz-Cabello J, Fuster V, Ibanez B, Bernal JA. Exercise triggers ARVC phenotype in mice expressing a disease-causing mutated version of human plakophilin-2. *J Am Coll Cardiol* 2015; **65**:1438–1450.
27. Hauswirth WW, Lewin AS, Zolotukhin S, Muzyczka N. Production and purification of recombinant adeno-associated virus. *Methods Enzymol* 2000; **316**:743–761.
28. Prasad KR, Xu Y, Yang Z, Toufektsian MC, Berr SS, French BA. Topoisomerase inhibition accelerates gene expression after adeno-associated virus-mediated gene transfer to the mammalian heart. *Mol Ther* 2007; **15**:764–771.
29. Xiao X, Li J, Samulski RJ. Production of high-titer recombinant adeno-associated virus vectors in the absence of helper adenovirus. *J Virol* 1998; **72**:2224–2232.
30. Roche-Molina M, Sanz-Rosa D, Cruz FM, Garcia-Prieto J, Lopez S, Abia R, Muriana FJ, Fuster V, Ibanez B, Bernal JA. Induction of sustained hypercholesterolemia by single adeno-associated virus-mediated gene transfer of mutant hPCSK9. *Arterioscler Thromb Vasc Biol* 2015; **35**:50–59.
31. Bao Y, Willis BC, Frasier CR, Lopez-Santiago LF, Lin X, Ramos-Mondragon R, Auerbach DS, Chen C, Wang Z, Anumonwo J, Valdivia HH, Delmar M, Jalife J, Isom LL. Scn2b deletion in mice results in ventricular and atrial arrhythmias. *Circ Arrhythm Electrophysiol* 2016; **9**:e003923.
32. Clasen L, Eickholt C, Angendohr S, Jungen C, Shin DI, Donner B, Furnkranz A, Kelm M, Klocker N, Meyer C, Makimoto H. A modified approach for programmed electrical stimulation in mice: inducibility of ventricular arrhythmias. *PLoS One* 2018; **13**:e0201910.
33. Cerrone M, Noujaim SF, Tolkacheva EG, Talkachou A, O'Connell R, Berenfeld O, Anumonwo J, Pandit SV, Vikstrom K, Napolitano C, Priori SG, Jalife J. Arrhythmogenic mechanisms in a mouse model of catecholaminergic polymorphic ventricular tachycardia. *Circ Res* 2007; **101**:1039–1048.
34. Macias AG-GA, Moreno-Manuel AI, Cruz FM, Gutiérrez LK, García-Quintás N, Roche-Molina M, Bermúdez-Jiménez FJ, Andrés V, Vera-Pedrosa ML, Martínez-Carrascoso I, Bernal JA, Jalife J. Kir2.1 dysfunction at the sarcolemma and the sarcoplasmic reticulum causes arrhythmias in a mouse model of andersen-tawil syndrome type 1. *Nature Cardiovascular Research* 2022; **1**:900–917.
35. Dhar Malhotra J, Chen C, Rivolta I, Abriel H, Malhotra R, Mattei LN, Brosius FC, Kass RS, Isom LL. Characterization of sodium channel alpha- and beta-subunits in rat and mouse cardiac myocytes. *Circulation* 2001; **103**:1303–1310.
36. Abriel H, Rougier JS, Jalife J. Ion channel macromolecular complexes in cardiomyocytes: roles in sudden cardiac death. *Circ Res* 2015; **116**:1971–1988.
37. Park SS, Ponce-Balbuena D, Kuick R, Guerrero-Serna G, Yoon J, Mellacheru D, Conlon KP, Basur V, Nesvizhskii AI, Jalife J, Rual JF. Kir2.1 interactome mapping uncovers PKP4 as a modulator of the Kir2.1-regulated inward rectifier potassium currents. *Mol Cell Proteomics* 2020; **19**:1436–1449.
38. Moreno C, Prieto P, Macias A, Pimentel-Santillana M, de la Cruz A, Traves PG, Bosca L, Valenzuela C. Modulation of voltage-dependent and inward rectifier potassium channels by 15-epi-lipoxin-A4 in activated murine macrophages: implications in innate immunity. *J Immunol* 2013; **191**:6136–6146.
39. Steinegger M, Meier M, Mirdita M, Vohringer H, Haunsberger SJ, Soding J. HH-suite3 for fast remote homology detection and deep protein annotation. *BMC Bioinformatics* 2019; **20**:473.
40. Song Y, DiMaio F, Wang RY, Kim D, Miles C, Brunette T, Thompson J, Baker D. High-resolution comparative modeling with RosettaCM. *Structure* 2013; **21**:1735–1742.
41. Vikstrom KL, Vaidyanathan R, Levinsohn S, O'Connell RP, Qian Y, Crye M, Mills JH, Anumonwo JM. SAP97 regulates Kir2.3 channels by multiple mechanisms. *Am J Physiol Heart Circ Physiol* 2009; **297**:H1387–H1397.
42. Whittaker DG, Ni H, El Harchi A, Hancox JC, Zhang H. Atrial arrhythmogenicity of KCNJ2 mutations in short QT syndrome: insights from virtual human atria. *PLoS Comput Biol* 2017; **13**:e1005593.
43. El Harchi A, McPate MJ, Zhang Y, Zhang H, Hancox JC. Action potential clamp and chloroquine sensitivity of mutant Kir2.1 channels responsible for variant 3 short QT syndrome. *J Mol Cell Cardiol* 2009; **47**:743–747.
44. Lopez-Izquierdo A, Ponce-Balbuena D, Ferrer T, Sachse FB, Tristani-Firouzi M, Sanchez-Chapula JA. Chloroquine blocks a mutant Kir2.1 channel responsible for short QT syndrome and normalizes repolarization properties in silico. *Cell Physiol Biochem* 2009; **24**:153–160.
45. Luo C, Wang K, Zhang H. Modelling the effects of chloroquine on KCNJ2-linked short QT syndrome. *Oncotarget* 2017; **8**:106511–106526.
46. Luo C, Wang K, Liu T, Zhang H. Computational analysis of the action of chloroquine on short QT syndrome variant 1 and variant 3 in human ventricles. *Annu Int Conf IEEE Eng Med Biol Soc* 2018; **2018**:5462–5465.
47. Dias-Melicio LA, Calvi SA, Bordon AP, Golim MA, Peracoli MT, Soares AM. Chloroquine is therapeutic in murine experimental model of paracoccidiodomycosis. *FEMS Immunol Med Microbiol* 2007; **50**:133–143.
48. Moore BR, Page-Sharp M, Stoney JR, Ilett KF, Jago JD, Batty KT. Pharmacokinetics, pharmacodynamics, and allometric scaling of chloroquine in a murine malaria model. *Antimicrob Agents Chemother* 2011; **55**:3899–3907.
49. Rodriguez-Menchaca AA, Navarro-Polanco RA, Ferrer-Villada T, Rupp J, Sachse FB, Tristani-Firouzi M, Sanchez-Chapula JA. The molecular basis of chloroquine block of the inward rectifier Kir2.1 channel. *Proc Natl Acad Sci U S A* 2008; **105**:1364–1368.
50. Arunachalam K, Alzahrani T. *Flecainide*. Treasure Island, FL: StatPearls; 2022.
51. Cerrone M, Noorman M, Lin X, Chkourko H, Liang FX, van der Nagel R, Hund T, Birchmeier W, Mohler P, van Veen TA, van Rijen HV, Delmar M. Sodium current deficit and arrhythmogenesis in a murine model of plakophilin-2 haploinsufficiency. *Cardiovasc Res* 2012; **95**:460–468.

52. Martin CA, Zhang Y, Grace AA, Huang CL. In vivo studies of Scn5a^{-/-} mice modeling Brugada syndrome demonstrate both conduction and repolarization abnormalities. *J Electrocardiol* 2010;**43**:433–439.
53. Alanis J, Gonzalez H, Lopez E. The electrical activity of the bundle of His. *J Physiol* 1958;**142**:127–140.
54. Yang J, Jan YN, Jan LY. Control of rectification and permeation by residues in two distinct domains in an inward rectifier K⁺ channel. *Neuron* 1995;**14**:1047–1054.
55. Kubo Y, Murata Y. Control of rectification and permeation by two distinct sites after the second transmembrane region in Kir2.1K⁺ channel. *J Physiol* 2001;**531**:645–660.
56. Dharmoon AS, Pandit SV, Sarmast F, Parisian KR, Guha P, Li Y, Bagwe S, Taffet SM, Anumonwo JM. Unique Kir2x properties determine regional and species differences in the cardiac inward rectifier K⁺ current. *Circ Res* 2004;**94**:1332–1339.
57. Melnyk P, Zhang L, Shrier A, Nattel S. Differential distribution of Kir2.1 and Kir2.3 subunits in canine atrium and ventricle. *Am J Physiol Heart Circ Physiol* 2002;**283**:H1123–H1133.
58. Panama BK, Lopatin AN. Differential polyamine sensitivity in inwardly rectifying Kir2 potassium channels. *J Physiol* 2006;**571**:287–302.
59. Panama BK, McLerie M, Lopatin AN. Heterogeneity of IK1 in the mouse heart. *Am J Physiol Heart Circ Physiol* 2007;**293**:H3558–H3567.
60. Varro A, Nanasi PP, Lathrop DA. Potassium currents in isolated human atrial and ventricular cardiocytes. *Acta Physiol Scand* 1993;**149**:133–142.
61. Yan DH, Nishimura K, Yoshida K, Nakahira K, Ehara T, Igarashi K, Ishihara K. Different intracellular polyamine concentrations underlie the difference in the inward rectifier K⁽⁺⁾ currents in atria and ventricles of the Guinea-pig heart. *J Physiol* 2005;**563**:713–724.
62. Medeiros-Domingo A, Kaku T, Tester DJ, Iturralde-Torres P, Itty A, Ye B, Valdivia C, Ueda K, Canizales-Quinteros S, Tusie-Luna MT, Makielski JC, Ackerman MJ. SCN4B-encoded sodium channel beta4 subunit in congenital long-QT syndrome. *Circulation* 2007;**116**:134–142.
63. Watanabe H, Darbar D, Kaiser DW, Jiramongkolchai K, Chopra S, Donahue BS, Kannankeril PJ, Roden DM. Mutations in sodium channel beta1- and beta2-subunits associated with atrial fibrillation. *Circ Arrhythm Electrophysiol* 2009;**2**:268–275.
64. Chen KH, Xu XH, Sun HY, Du XL, Liu H, Yang L, Xiao GS, Wang Y, Jin MW, Li GR. Distinctive property and pharmacology of voltage-gated sodium current in rat atrial vs ventricular myocytes. *Heart Rhythm* 2016;**13**:762–770.
65. Edokobi N, Isom LL. Voltage-Gated sodium channel beta1/beta1B subunits regulate cardiac physiology and pathophysiology. *Front Physiol* 2018;**9**:351.
66. Angsutararux P, Zhu W, Voelker TL, Silva JR. Molecular pathology of sodium channel Beta-subunit variants. *Front Pharmacol* 2021;**12**:761275.
67. Li GR, Lau CP, Shrier A. Heterogeneity of sodium current in atrial vs epicardial ventricular myocytes of adult Guinea pig hearts. *J Mol Cell Cardiol* 2002;**34**:1185–1194.
68. Holmes AP SOB, Johnson DM, Kabir SN COS, Avezza A MOR, Reyat JS, Hall AW, Apicella C, Ellinor PT, Niederer S, Tucker NR, Fabritz L, Kirchhof P, Pavlovic D. Increased atrial effectiveness of flecainide conferred by altered biophysical properties of sodium channels. *J Mol Cell Cardiol* 2022;**166**:23–35.
69. Anumonwo JM, Tallini YN, Vetter FJ, Jalife J. Action potential characteristics and arrhythmogenic properties of the cardiac conduction system of the murine heart. *Circ Res* 2001;**89**:329–335.
70. Herron TJ, Milstein ML, Anumonwo J, Priori SG, Jalife J. Purkinje cell calcium dysregulation is the cellular mechanism that underlies catecholaminergic polymorphic ventricular tachycardia. *Heart Rhythm* 2010;**7**:1122–1128.
71. Kang G, Giovannone SF, Liu N, Liu FY, Zhang J, Priori SG, Fishman GI. Purkinje cells from RyR2 mutant mice are highly arrhythmogenic but responsive to targeted therapy. *Circ Res* 2010;**107**:512–519.
72. Vaidyanathan R, O'Connell RP, Deo M, Milstein ML, Furspan P, Herron TJ, Pandit SV, Musa H, Berenfeld O, Jalife J, Anumonwo JM. The ionic bases of the action potential in isolated mouse cardiac purkinje cell. *Heart Rhythm* 2013;**10**:80–87.
73. Park MH, Igarashi K. Polyamines and their metabolites as diagnostic markers of human diseases. *Biomol Ther (Seoul)* 2013;**21**:1–9.
74. Willis BC, Ponce-Balbuena D, Jalife J. Protein assemblies of sodium and inward rectifier potassium channels control cardiac excitability and arrhythmogenesis. *Am J Physiol Heart Circ Physiol* 2015;**308**:H1463–H1473.
75. Weidmann S. The effect of the cardiac membrane potential on the rapid availability of the sodium-carrying system. *J Physiol* 1955;**127**:213–224.
76. Kleber AG. The shape of the electrical action-potential upstroke: a new aspect from optical measurements on the surface of the heart. *Circ Res* 2005;**97**:204–206.
77. Gee SH, Madhavan R, Levinson SR, Caldwell JH, Sealock R, Froehner SC. Interaction of muscle and brain sodium channels with multiple members of the syntrophin family of dystrophin-associated proteins. *J Neurosci* 1998;**18**:128–137.
78. Gillet L, Rougier JS, Shy D, Sonntag S, Mougnot N, Essers M, Shmerling D, Balse E, Hatem SN, Abriel H. Cardiac-specific ablation of synapse-associated protein SAP97 in mice decreases potassium currents but not sodium current. *Heart Rhythm* 2015;**12**:181–192.
79. Leonoudakis D, Mailliard W, Wingerd K, Clegg D, Vandenberg C. Inward rectifier potassium channel Kir2.2 is associated with synapse-associated protein SAP97. *J Cell Sci* 2001;**114**:987–998.
80. Petitprez S, Zmoos AF, Ogrodnik J, Balse E, Raad N, El-Haou S, Albesa M, Bittihn P, Luther S, Lehnart SE, Hatem SN, Coulombe A, Abriel H. SAP97 and dystrophin macromolecular complexes determine two pools of cardiac sodium channels nav1.5 in cardiomyocytes. *Circ Res* 2011;**108**:294–304.
81. Vaidyanathan R, Taffet SM, Vikstrom KL, Anumonwo JM. Regulation of cardiac inward rectifier potassium current (I(K1)) by synapse-associated protein-97. *J Biol Chem* 2010;**285**:28000–28009.
82. Hu D, Barajas-Martinez H, Medeiros-Domingo A, Crotti L, Veltmann C, Schimpf R, Urrutia J, Alday A, Casis O, Pfeiffer R, Burashnikov E, Caceres G, Tester DJ, Wolpert C, Borggrefe M, Schwartz P, Ackerman MJ, Antzelevitch C. A novel rare variant in SCN1Bb linked to brugada syndrome and SIDS by combined modulation of na(v)1.5 and K(v)4.3 channel currents. *Heart Rhythm* 2012;**9**:760–769.
83. Epstein JA, Franklin H. Epstein lecture. Cardiac development and implications for heart disease. *N Engl J Med* 2010;**363**:1638–1647.
84. Wu TJ, Yashima M, Xie F, Athill CA, Kim YH, Fishbein MC, Qu Z, Garfinkel A, Weiss JN, Karagueuzian HS, Chen PS. Role of pectinate muscle bundles in the generation and maintenance of intra-atrial reentry: potential implications for the mechanism of conversion between atrial fibrillation and atrial flutter. *Circ Res* 1998;**83**:448–462.
85. Iacobas S, Amuzescu B, Iacobas DA. Transcriptomic uniqueness and commonality of the ion channels and transporters in the four heart chambers. *Sci Rep* 2021;**11**:2743.
86. Gaborit N, Le Bouter S, Szuts V, Varro A, Escande D, Nattel S, Demolombe S. Regional and tissue specific transcript signatures of ion channel genes in the non-diseased human heart. *J Physiol* 2007;**582**:675–693.

Translational perspective

The pathologic genetic variation of the strong inward rectifier K⁺ channel (Kir2.1^{E299V}) leads to SQT3S with atrial-specific arrhythmias while paradoxically enhancing Purkinje fiber excitability and ventricular conduction velocity. The availability of an animal model of SQT3S may lead to the identification of new molecular targets in the design of novel drugs to treat a cardiac disease that currently has no defined therapy. The chemical skeleton of polyamines, which block Kir2.1 channels at specific voltages, may serve as a template for designing new drugs capable of correcting hyperfunctional Kir2.1 channels, and preventing arrhythmias in SQT3S and possibly other diseases.